Winkler, Stefan, Matthews, John A, Haselberger, Stefan, Hill, Jennifer ORCID logoORCID: https://orcid.org/0000-0002-0682-783X, Mourne, Richard W, Owen, Geraint and Wilson, Peter (2020) Schmidt-hammer exposure-age dating (SHD) of sorted stripes on Juvflye, Jotunheimen (central South Norway): Morphodynamic and palaeoclimatic implications. Geomorphology, 353. p. 107014. doi:10.1016/j.geomorph.2019.107014

Schmidt-hammer exposure-age dating (SHD) of sorted stripes on Juvflye, Jotunheimen (central South Norway): Morphodynamic and palaeoclimatic implications

Stefan Winkler[1], John A. Matthews[2], Stefan Haselberger[3], Jennifer L. Hill[4], Richard W. Mourne[5], Geraint Owen[2], Peter Wilson[6]

(1) Department of Geography and Geology, Julius-Maximilians-University Würzburg, Germany

(2) Department of Geography, Swansea University, Wales, UK

(3) Department of Geography, University of Vienna, Austria

(4) Academic Development Unit, University of Gloucestershire, Cheltenham, UK

(5) Department of Geography and Environmental Management, University of the West of England, Bristol, UK

(6) School of Geography and Environmental Sciences, Ulster University, Coleraine, Northern Ireland, UK

Corresponding author: Stefan Winkler

E-mail address: stefan.winkler@uni-wuerzburg.de

Postal address: Department of Geography and Geology, Julius-Maximilians-University Würzburg, Am Hubland, D-97074 Würzburg, Germany

Abstract

Measurements with an electronic Schmidt-hammer (RockSchmidt) were conducted on 23 sites of sorted stripes (periglacial patterned ground) on Juvflye, Jotunheimen (central South Norway). All were located above the current lower limit of alpine permafrost. Performing Schmidt-hammer

exposure-age dating (SHD) based on application of a new local age-calibration equation for R_{Rock}-values yielded SHD-ages between 7,975 ± 370 and 6,660 ± 355 years ago, which are closely comparable to results obtained previously from sorted circles at the same location. The age estimates are interpreted as 'composite' ages indicative of upfreezing of boulders, lateral sorting, and subsequent stabilisation. Formation of patterned ground essentially ceased with the onset of the regional Holocene Thermal Maximum (HTM). Neither sorted stripe sites at higher altitude, continuously underlain by permafrost during the entire Holocene, nor those at lower altitudes affected by re-aggradation of permafrost in the late Holocene show signs of significant recent morphodynamic activity. Likely explanations for early- to mid-Holocene stabilisation include (1) substantial changes of soil moisture conditions and related thermodynamics within the active layer affecting frost action, (2) loss of fine-grained substrate matrix from the coarse stripes and hence reduced frost susceptibility, and (3) exhaustion of supply of boulders from the fines-dominated areas. Whereas the sorted stripe data set as a whole did not reproduce the altitudinal gradient characteristic of sorted circles on Juvflye, the strength of the relationship between sorted stripe mean R_{Rock}-values and altitude increased with declining slope gradient. Although interpretation of SHD-ages for patterned ground remains challenging, this successful application of the electronic Schmidt-hammer, with its increased efficiency and technical improvements over the mechanical Schmidt-hammer, offers considerable potential for future SHD-studies in both morphodynamic and palaeoclimatic contexts.

Keywords:

Periglacial patterned ground, sorted stripes, alpine permafrost, Schmidt-hammer exposure-age dating (SHD), RockSchmidt, Holocene palaeoclimatology

Highlights:

• Successful application of the electronic Schmidt-hammer (RockSchmidt) for SHD

• Stabilisation of sorted stripes around onset of regional Holocene Thermal Maximum

• Good correspondence of ages for sorted stripes with previously studied sorted circles

• Indication of relationship between sorted stripe age and altitude on low angle slopes

• No substantial late Holocene morphodynamic activity despite underlying permafrost

1. Introduction

The periglacial process system and its landforms constitute an important element of temperate and subpolar mountain regions (Caine, 1974; Harris, 1988; Thompson, 1990; Slaymaker and Embleton-Hamann, 2018). Mountain permafrost is part of the alpine cryosphere and its past, present, and predicted future changes in distribution and thermal conditions have implications for a wide spectrum of related issues (Harris et al., 2009; Slaymaker and Embleton-Harris, 2009; Barry and Gan, 2011; Beniston et al., 2018). Close causal relationships between permafrost and many periglacial landforms explain why the latter have for a long time been utilised as palaeoclimatic indicators (Washburn, 1979; Büdel, 1981; Ballantyne and Harris, 1994; Matsuoka, 2011; Ballantyne, 2018; French, 2018). Among numerous attempts to utilise periglacial landforms for palaeoclimatic research in mountain regions, both investigation of the transition between glacial and periglacial process systems (e.g. Matthews et al., 2017) and the collection of supportive data for constraints on Late Glacial and early Holocene glacier chronologies (Böhlert et al., 2011a) have recently gained attention. A major barrier in this context, however, is the application of suitable dating techniques. Many periglacial landforms are boulder-dominated and experience formation by continuous processes rather than by singular events. This restricts possible application of numerical dating techniques such as radiocarbon (^{14}C) dating or terrestrial cosmogenic nuclide exposure-age dating (TCND), the former due to sparsity of organic matter, the latter essentially because of financial, logistic, or conservational limitations on sample quantity.

Following its introduction to geomorphology five decades ago (McCarroll, 1994; Goudie, 2006), the Schmidt-hammer has successfully been applied for the purpose of relative-age dating of boulder and

bedrock surfaces (e.g. Matthews and Shakesby, 1984; McCarroll, 1989; Nesje et al., 1994a,b; Evans et al., 1999; Aa and Sjåstad, 2000; Winkler, 2005; Kellerer-Pirklbauer et al., 2008; Klapyta, 2013). More recently, its combination with numerical age dating, especially surface exposure-age dating utilising cosmogenic radionuclides such as [10]Be, has enabled the calculation of age-calibration equations, the emergence of Schmidt-hammer exposure-age dating (SHD) as a successful calibrated-age dating technique, and its application to an increasing range of different landforms. The latter includes, for example, moraines (Winkler 2009, 2014; Matthews and Winkler, 2011; Tomkins et al., 2016, 2018a), rock slope failures (Matthews et al., 2018; Wilson et al., 2019), rock glaciers (Böhlert et al., 2011b; Rode and Kellerer-Pirklbauer, 2011; Matthews et al., 2013; Winkler and Lambiel, 2018), block streams (Wilson et al., 2017), block fields (Marr et al., 2018), patterned ground (Winkler et al., 2016), cryoplanation terraces (Matthews et al., 2019), ice-cored moraines (Matthews et al., 2014), pronival ramparts (Matthews et al., 2011, 2017; Matthews and Wilson, 2015), and snow-avalanche impact ramparts (Matthews et al., 2015). The advantages of SHD for surface-exposure age dating of boulder-rich landforms with diachronous surfaces or land surfaces potentially affected by postdepositional disturbance place it in an outstanding position among other dating techniques.

The mountain region of Jotunheimen in central South Norway is characterised by a variety of periglacial landforms. Its geological history and gross morphology are responsible for a rather specific periglacial process-system and altitudinal zonation of landforms. Unlike many temperate or subpolar mountain ranges, blockfields and different types of patterned ground are omnipresent whereas other typical periglacial features (e.g. rock glaciers) are rare. A recent review by Winkler et al. (2020) highlights these differences and demonstrates that, apart from regional permafrost studies or special topics such as micro-scale features on recently deglaciated terrain, there is still much potential for in-depth investigation into the periglacial landsystem in Jotunheimen, in particular its chronological constraints and palaeoclimatic context.

In a previous application of SHD to sorted circles on Juvflye, a high-altitude plateau in central Jotunheimen, Winkler et al. (2016) demonstrated that this type of patterned ground stabilised during the early Holocene Thermal Maximum (HTM). The sorted circles were largely unaffected by late-

Holocene climate deterioration and no appreciable recent morphodynamic activity was reported. These findings are of palaeoclimatic significance and have morphodynamic implications. Various studies confirm that most of the patterned ground on Juvflye is still currently underlain by deep permafrost and sites located at higher altitude remained so during the entire Holocene including the HTM (see 2.2). This raises questions about the role of permafrost in patterned ground formation and in accounting for recent inactivity. Processes of periglacial patterned ground formation are, however, complex (see Washburn, 1956, 1979; Corte, 1963; Goldthwait, 1976; French, 1988; Hallet et al., 1988; Williams and Smith, 1989; Hallet, 1990, 2013; Van Vliet-Lanoë, 1991; Kessler et al., 2001; Matsuoka et al., 2003; Ballantyne, 2013, 2018; Warburton, 2013). Research on periglacial patterned ground has mainly focused on sorted/nonsorted circles and polygons, with studies on sorted stripes being less common (e.g. Ball and Goodier, 1968; Hall, 1983; Ballantyne, 2001, Francou et al., 2001). In addition to processes related to repeated freezing and thawing within the active layer on flat terrain, a downslope component of periglacial mass wasting needs to be considered in sorted stripe formation (Mackay and Mathews, 1974; Williams and Smith, 1989; Werner and Hallet, 1993; Ballantyne and Harris, 1994; Ballantyne, 2018; Li et al., 2018).

Although Winkler and Matthews (2014) demonstrated that data obtained by mechanical and electronic Schmidt-hammers are interconvertible and Winkler et al. (2016) subsequently applied both instruments in the field, all regional SHD-calibration equations to date have been derived for mechanical Schmidt-hammers. To fully assess the utility of the recently introduced electronic Schmidt-hammer (RockSchmidt) in Jotunheimen, the calculation of individual calibration equations for the new instrument remains essential. This task is attempted here as one of the research objectives of the current study, which can be summarized as follows:

• Investigate the potential morphological, sedimentological, and topographical controls on Schmidt-hammer data from sorted stripes;

• Establish a local SHD-calibration equation for electronic Schmidt-hammers and apply it to the sorted stripes;

• Assess the morphodynamic and palaeoclimatic implications of the SHD-age of sorted stripes with particular reference to the altitudinal variation of permafrost during the Holocene;

• Compare the results from the sorted stripes with those previously obtained from sorted circles at the same location.

2. Study area

2.1. Location, geology, and geomorphology

Jotunheimen in central South Norway constitutes a part of the Scandinavian Caledonides. It covers approximately 3500 km^2 and is home to the highest peak in Norway (Galdhøpiggen, 2469 m a.s.l.). Its geological history (Fossen et al., 2008) is responsible for the characteristic modern topography with widespread high-altitude plateaus classified as 'high paleic mountains with glacial incision, mostly moderate slopes' (Etzelmüller et al. 2007). Our study area, Juvflye, is a high-level plateau in central Jotunheimen (Figs. 1,2a,b). Its central part is flat to gently sloping terrain covering 8 – 10 km^2 at altitudes between 1850 and 1950 m a.s.l. Juvflye and similar plateaus are traditionally interpreted as relict, pre-glacial landforms summarised by the term 'paleic surface' (Reusch, 1901; Ahlmann, 1919; Gjessing, 1967, 1978; Nesje and Whillans, 1994; Lidmar-Bergström et al., 2000; see Winkler et al. 2020 for details).

Lithologically, the high-grade metamorphic rocks of central Jotunheimen are dominated by pyroxene-granulite gneiss (Battey and Bryhni, 1981; Sigmond et al., 1984). This also applies to the composition of till on Juvflye in which the investigated patterned ground has developed. Several other lithologies, including gabbroic gneiss, mylonitic gneiss, amphibolite, and peridotite, occur sporadically throughout the region (Lutro and Tveten 1996). Consequently, few boulders of these different bedrock types occur in the till. However, the dominant pyroxene-granulite gneiss is lithologically and mineralogically comparatively homogeneous (Battey and McRitchie, 1973, 1975) and has supported previous application of regional Schmidt-hammer calibration equations (Matthews and Owen, 2010; Matthews and Winkler, 2011; Matthews et al., 2014, 2018). It should be noted that both the lithology of glacially-scoured bedrock selected as one 'old' control point (see

3.3) and the boulders sampled from the sorted stripes showed no notable 'mylonitic' characteristics (cf. Matthews et al., 2019).

As a result of its specific gross morphology with moderate slopes and extensive plateau surfaces, patterned ground covers ~47 % and blockfields ~38 % of the entire periglacial zone in Jotunheimen (Donner, 2019). This dominance is unusual for mid-latitudinal mountain ranges and justifies the focus on Juvflye as typical of high-level plateaus where different varieties of patterned ground occur. Ødegård et al. (1987, 1988) present a detailed geomorphological map of Juvflye and estimate that 20 to 50% of the area of continuous till cover above 1750 m a.s.l. with slope gradients of <10° shows patterned ground. Patterned ground cover attains its maximum spatial extent between 1900 and 1950 m a.s.l. (up to 50%) but remains at levels >30 % between 1800 and 2000 m a.s.l. Ødegård et al. (1987, 1988) follow the classification of patterned ground by Washburn (1956, 1979) and report that sorted polygons, nets, and circles are typical for flat terrain (~0° – 6°, average 2.0°). By contrast, sorted steps (~2° – 11°, average 3.9°) and sorted stripes (~3° – 17°, average 7.3°) dominate on shallow to moderate slope gradients (Figs. 2,3). Especially at the northern rim of Juvflye, on slope gradients exceeding 12°, areas of sorted stripes are frequently bound by boulder tongues at their downslope end (Fig. 2c,f). It should be noted that Ødegård et al. (1988) mention the 'fossil' appearance of patterned ground and that their observation provided Winkler et al. (2016) with an inducement to apply SHD to sorted circles on Juvflye.

2.2. Climate, permafrost, and palaeoclimatology

The meteorological station at the summit of Juvasshøe (1894 m a.s.l.; Fig. 1) reports a mean annual air temperature (MAAT) of −3.4°C for its operational period since 1999 and a calculated MAAT of -4.6°C for the normal period 1961-90 (www.met.no). Previously, Ødegård et al. (1992) calculated MAATs ranging from -2.6°C at 1500 m a.s.l. to -6.4°C at 2200 m a.s.l. on Juvflye based on data from 11 meteorological stations around Jotunheimen. These values correspond well to 1 km-gridded MAAT normals 1971-2000 of between -2.0 and -4.0°C (www.senorge.no). Mean monthly air temperatures for Juvasshøe are presented in Tab. 1 whereas annual mean air temperatures vary between −2.5°C (2014) and −5.4°C (2010; www.met.no). Estimates for annual precipitation at Juvflye

range from 800 to 1000 mm (Farbrot et al., 2011), but detailed data are not available. The 1 km-gridded mean annual precipitation normals show slightly higher values (www.senorge.no). Ødegård et al. (1992) mention, however, that strong winds typical for Juvflye result in comparatively little snow cover with a (late) maximum snow depth of 0.5 m in May.

Jotunheimen constitutes a major permafrost region within Scandinavia (Gisnås et al., 2013, 2017) and both its condition and altitudinal distribution on Juvflye are well established. Based on MAAT calculations, Ødegård et al. (1992, 1996) estimate the altitudinal lower limit of alpine permafrost around Juvflye at ~1450 m a.s.l. They report a mean annual ground temperature (MAGT) for Galdehøe (2195 m a.s.l.) of -4.2 to -4.4°C, for a site near Juvvatnet (1855 m a.s.l.) of -1.7 to -1.9°C, and for Dugurdskampen (1547 m a.s.l.) of -0.6 to -0.7°C. Their lower limit of alpine permafrost at 0°C MAGT is equivalent to a MAAT of about -2.5°C. Farbrot et al. (2011) show, however, that the difference between MAAT and MAGT can vary between <1°C for exposed, bare sites and up to 4.5°C for sites experiencing prolonged snow cover (cf. Kade et al., 2006). Based on geophysical measurements, Isaksen et al. (2002) place the lower limit of alpine permafrost on Juvflye at 1460 m a.s.l., whereas Hauck et al. (2004) place it in a zone between 1410 and 1470 m a.s.l. Farbrot et al. (2011) measure MAGT at 10 m depths along a borehole-transect on Juvflye and calculate an altitudinal gradient of -0.005°C/m^{-1}. Five boreholes at altitudes between 1559 and 1894 m a.s.l. show MAGTs between -0.3 and -2.5°C and indicate permafrost. At two additional boreholes on the northern slope of Juvflye (1307 and 1458 m a.s.l.) only seasonal frost was detected. Isaksen et al. (2001) calculate a total thickness of permafrost of ~380 m at Juvvasshøe based on data from a 129 m deep borehole. Ødegård et al. (1999) postulate that permafrost at altitudes between 1600 and 1450 m a.s.l. on the slopes of Juvflye is degrading and at 1600 m a.s.l. restricted to a depth below 20 m. For central Juvflye an active layer thickness range between 1.95 and 2.45 m is reported by Harris et al. (2009). Current and future climate change will, however, affect the properties of permafrost, in particular near-surface temperatures, active layer depth, and altitudinal lower limits (Isaksen et al., 2007, 2011; Hipp et al., 2012).

Central Jotunheimen and Juvflye are located close to former centres of the Late Pleistocene Scandinavian Ice Sheets (Mangerud et al., 2011). High-resolution ice-sheet modelling (Patton et al.,

2016) indicates that large parts of Jotunheimen, including its high-altitude plateaus, were likely covered by cold-based, low-velocity ice with limited erosional potential during long periods of the last glaciation. Ice-streams with high erosional potential and different basal conditions existed only in topographically-confined valleys. Unfortunately, there is no detailed information about when Juvflye and surrounding valleys were deglaciated. General chronological reconstructions agree on final regional deglaciation ~10 kyr ago (Hughes et al., 2016; Stroeven et al., 2016; Patton et al., 2017). Furthermore, regionally focused studies infer that deglaciation around Juvflye and in the surrounding valleys likely occurred after the 'Erdalen event' at c. 9700 cal. a BP (Dahl et al., 2002; Matthews and Dresser, 2008; Matthews et al., 2018).

Holocene variability of permafrost in Jotunheimen has been much less studied than its glacier chronology (cf. Matthews and Dresser, 2008, Winkler et al., 2020, and references therein). An exception is the reconstruction of variations in altitudinal permafrost limits by Lilleøren et al. (2012) based on air temperature series from various proxy sources for the past 10,000 years. They utilised the proxy evidence to drive a one-dimensional heat-flow model and a new equilibrium permafrost model (Gisnås et al., 2013). After calibration with existing borehole-temperature data (see above), Lilleøren et al. (2012) conclude that permafrost existed at the highest altitudes in Jotunheimen during the entire Holocene. However, large permafrost areas degraded during the Holocene Thermal Maximum (HTM). Their model indicates re-aggradation of permafrost since termination of the HTM and maximum permafrost extent during the 'Little Ice Age' (LIA). Based on this reconstruction it can be assumed that on Juvflye only terrain above c. 1850 m a.s.l. experienced continuous permafrost during the HTM. In the zone below (down to c. 1650-1700 m a.s.l.) permafrost is likely to have survived only below superficial taliks. Thus, post-HTM development of permafrost on Juvflye affected the altitudinal zone between 1650/1700 and 1400 m a.s.l., which again faced degradation following the LIA. Lilleøren et al. (2012) suggested that at c. 1560 m a.s.l. permafrost disappeared around 8.0 - 7.8 kyr ago. This age corresponds remarkably well to the ages provided by Winkler et al. (2016) for the stabilisation of sorted circles at the same location (8,050 ± 560 years ago for a site at 1550 m a.s.l.).

3. Methodology

3.1. Geomorphological field measurements and observations

Based on aerial photography, the geomorphological map of Ødegård et al. (1987), and previous fieldwork, our selection of sites aimed at covering a representative range of altitudes, aspects, and specific morphologies of sorted stripes. Relevant morphological information for the selected sorted stripe sites was collected during fieldwork and topographical data (altitude and aspect) was cross-checked against topographic maps. Width and length of coarse stripes targeted for sampling with the RockSchmidt were measured with tape and laser rangefinder. Additionally, the width of fine-grained terrain between the parallel coarse stripes (i.e. their horizontal spacing) was measured. The measurements of coarse stripe width and horizontal spacing were usually conducted in their lower (downslope) and upper (upslope) sectors, and subsequently averaged. Morphological observations focused on any visual signs of disturbance indicating recent morphodynamic activity, such as cryoturbation or solifluction.

At all sorted stripe sites average and maximum boulder length was estimated and 100 boulders from each site were assessed for their roundness following the visual comparison method of Powers (1953). The aim was to detect possible sedimentological differences in the substrate and determine potential effects on stripe morphology and R_{Rock}-values. The clast roundness data was qualitatively analysed and quantitatively compared using a numerical index of mean roundness (*ir*) assigning numerical values to each roundness class (very angular, 0.5; angular, 1.5 … to well rounded, 5.5; cf. Powers, 1953; Matthews, 1987; Tucker, 1988).

3.2. Schmidt-hammer measurements

Schmidt-hammer measurements at the 23 selected sorted stripe sites (Fig. 1) were performed in summer 2019 by a single operator. Sampling was restricted to boulders in the coarse stripes as the fine-grained terrain between coarse stripes is commonly free of larger clasts (Fig. 3). Sampling was conducted consistently along individual coarse stripes at each site and suitable boulders were tested

in a non-selective fashion. Schmidt-hammer impacts were performed on lichen-free surface areas of boulders and any visible cracks or weaknesses were avoided. A requirement for accepted tests was that boulders did not move on impact. Average boulder long axes were 35 – 40 cm at the sites (a few large boulders reached 100 - 310 cm). All boulders were tested with one single impact. Sparsity of larger boulders prevented the application of sampling designs involving multiple impacts per boulder. Furthermore, the sampling design ensures comparability with the sorted circle data of Winkler et al. (2016).

A total of 400 individual boulders, divided into 20 subsamples of 20 boulders each, was tested at every site. The high number of subsamples was chosen to allow detection of possible patterns within stripes. Accordingly, the detailed location of every subsample in relation to individual stripes was recorded during Schmidt-hammer sampling. Following successful application during previous fieldwork in Jotunheimen (Winkler and Matthews, 2014; Winkler et al., 2016), measurements were carried out using the recently introduced electronic RockSchmidt (N-Type configuration) with an impact energy of 2.207 Nm for its plunger (Proceq, 2014). Because the compressional strength/surface hardness registered after impact of the plunger is measured differently compared to a mechanical Schmidt-hammer, RockSchmidt R(Rebound)-values are not affected by the instrument angle relative to the ground. It was, therefore, not necessary to restrict Schmidt hammer impacts to horizontal or near-horizontal upper surfaces of boulders. Although R-values obtained with electronic and mechanical Schmidt-hammers have been demonstrated to be interconvertible (Winkler and Matthews, 2014), absolute values are not identical. To avoid confusion with R-values reported by previous studies in the region, the term 'R_{Rock}-value' is used throughout this paper for the RockSchmidt data. The instrument was tested on a manufacturer's test anvil before and after measurements to ensure consistent calibration. Detailed R_{Rock}-value data from these calibration tests were retained to enable possible corrections for differences of instrument performance within the calibration window specified by the manufacturer. Where necessary, such corrections were performed applying a correction factor based on the anvil test data to all individual R_{Rock}-values as recommended (Proceq, 2014). All RockSchmidt data utilised in this study including those obtained during previous fieldwork are consequently free from any instrumental bias (see 5.1).

Ultimately, the data collected at each sorted stripe site were treated as a homogeneous sample during data analysis. Sample R_{Rock}-values means and their 95 % confidence intervals ($\alpha = 0.05$) were calculated following established procedures (following Shakesby et al., 2006). Because the sorted stripes do not constitute landforms related to single/short-term events, histograms have been produced for all sites to visually assist interpretation of the spread of R_{Rock}-values in terms of diachronous surface exposure. For the same purpose, statistical analyses including Kolmogorov-Smirnov tests for normality (Schönwiese, 1992; Sachs, 1999) were performed.

3.3. Schmidt-hammer exposure-age dating (SHD)

Since Winkler and Matthews (2014) previously demonstrated that mechanical and electronic Schmidt-hammer data are interconvertible, all R_{Rock}-values obtained here could theoretically be converted and subsequently existing calibration equations based on mechanical Schmidt-hammer R-values applied. However, it was decided to establish a new, independent calibration equation for the RockSchmidt based on local control points. Previous attempts (Matthews et al., 2014; Winkler et al., 2016; Matthews et al., 2019) have, however, shown that it is no trivial task to establish suitable and reliable control points on Juvflye, mainly due to the lack of glacially-scoured bedrock exposures and surfaces of known numerical age.

Several different surfaces have been used previously in the area as control points. As the 'young' control point, Matthews et al. (2019) used a fresh, unweathered bedrock cliff associated with an active cryoplanation terrace. But both local lithology (mylonitised gneiss) and the geomorphological context leave this site less suitable for use in the current study. Winkler et al. (2016) used freshly exposed boulders at road-cuts on the northern slope of Juvflye and adopted a multiple impact approach on identical impact spots (cf. Poole and Farmer, 1980) to obtain R-values representative of unweathered bedrock. Boulders on the recent glacier foreland of Vesljuvbrean served as the 'young' control point for Matthews et al. (2014), with aerial photography allowing an age estimate of c. 50 years for their exposure. Because recent construction activity at Galdhøpiggen Summerskisenter resulted in fresh exposure of boulders within a few tens of metres of the current

glacier margin of Vesljuvbrean (Figs.1,2b), two sites within this locality (y1/2) were selected as the 'young' control point for this study.

Glacially-scoured bedrock exposed during deglaciation assumed to have taken place ~ 9.7 kyr ago (see 2.2), served as the 'old' control point for both Matthews et al. (2014) and Winkler et al. (2016). These surfaces (x2 on Fig.1) were re-sampled with a RockSchmidt in 2017. Three sections of a high-altitude terminal moraine on the north-eastern slope of Juvflye (c. 1650 m a.s.l.; x1.1 – x1.3 on Fig. 1) were sampled in 2019 and used as the 'old' control point for this study. The moraine is assumed to date from the Erdalen Event (~10 kyr ago), the conventional last local ice-sheet re-advance followed by final deglaciation (cf. Matthews et al., 2018). In addition to this new local calibration equation, a new regional calibration equation for the RockSchmidt was calculated based on R_{Rock}-values from Winkler and Matthews (2014), who re-sampled 'young' and 'old' control point sites originally utilised by Matthews and Owen (2010) for their regional SHD-calibration equations for Jotunheimen.

The procedure for calculating SHD-calibration equations based on the RockSchmidt data obtained here followed established practice for high-precision SHD explained in detail by Matthews and Owen (2010), Matthews and Winkler (2011), and Matthews and McEwen (2013). In their fundamental work at an ideal study site, Shakesby et al. (2011) confirmed that the R-value-age relationship can best be described by a linear function. Other studies in Jotunheimen (e.g. Matthews et al., 2014, 2018, 2019; Winkler et al., 2016) and elsewhere (Winkler, 2014; Tomkins et al., 2018a,b; Winkler and Lambiel, 2018) reached similar conclusions for Holocene and Late Glacial timescales and for comparable resistant types of bedrock. Based on at least one 'old' and one 'young' control point with independent age information, the SHD-calibration equation follows the standard equation for linear regression:

$$y = a + bx \tag{1}$$

where y = surface age in years, x = mean R_{Rock}-value, a = intercept age, and b = slope of the calibration curve.

Confidence intervals for the final SHD-age estimates reflect the total error (C_t), which combines the sampling error of the sorted stripe sites (C_s) with the error of the calibration curve (C_c) following Matthews and Winkler (2011):

$$C_t = \sqrt{(C_s{}^2 + C_c{}^2)}. \tag{2}$$

C_s is derived from the slope of the calibration curve (b), Student's t statistic and the standard error of the mean R-value of the sites, where s is the standard deviation and n is the sample size (Matthews and Owen, 2010):

$$C_s = \pm\, b\, [ts/\sqrt{(n\text{-}1)}] \tag{3}$$

C_c is derived from the confidence intervals associated with the 'old' control point (C_o) and the 'young' control point (C_y), where R_o, R_y and R_s are the mean R_{Rock}-values of these two control points and the sampled sites, respectively (Matthews and McEwen, 2013):

$$C_c = C_o - [(C_o - C_y)(R_s - R_o)/(R_y - R_o)]. \tag{4}$$

4. Results

4.1. Geomorphological measurements and observations

Average slope gradients at the sorted stripe sites investigated range between 5° and 22° (Tab. 2) and correspond to the data provided by Ødegård et al. (1988; see 2.1). The sorted stripe sites selected for investigation show some morphological variation (Fig. 3). Even within sites the width of individual course stripes can vary considerably. Whereas some stripes widen slightly downslope, others narrow or show consistent width. The distance between coarse stripes, i.e. the largely boulder-free and vegetated area dominated by finer grain sizes, always exceeds the width of adjacent coarse stripes, sometimes by three-times or more. Coarse stripes typically measure many tens of metres in length with a few exceeding 100 metres. Many coarse stripes are straight and parallel in accordance with the inclination of the slope, others curve (Fig. 2e,f,g). At some sites, especially those with lower slope gradients, individual stripes may bifurcate or converge with

adjacent stripes (Fig. 2d). More rarely, stripes exhibit a sinuous pattern with gradual transitions from sorted steps and circles upslope (Fig. 2f,g).

The results of the clast roundness measurements (Tab. 2) allow two groups to be recognised. The majority of the sites (18) have a dominant subangular clast category, a secondary peak in the subrounded category, and roundness index (*ir*) values between 2.81 and 2.30. This *ir*-range and the corresponding clast category distributions are similar to the results from sorted circles on Juvflye. Five sites (Juv 2+3, 14-16) exhibit maxima within the angular clast category and yield lower values for their *ir* of between 1.80 and 1.68. The latter group of sites surround Juvhøe (Fig. 1) at relatively high altitude (1830 – 1865 m a.s.l.) and lie close to the boundary between till and *in situ*-weathered material covering the summit of Juvhøe as mapped by Ødegård et al. (1987). A higher percentage of very angular and angular *in situ*-weathered clasts is the likely explanation for this difference in clast roundness because no general relationship between *ir* and altitude can be detected in the data for all sites (see below). The dominant subangular nature of surface material at the majority of sites is regarded as typical for tills in mountain environments (Evans and Benn, 2004; Lukas et al., 2013). Its limited variability seems not to have influenced the R_{Rock}-data (Fig. 8).

All signs of recent morphodynamic activity observed during SHD-sampling are limited to the fine-grain sedimentary material between individual coarse stripes. Circular and slightly elongated areas of bare fine-grained substrate with diameters of 30 to 50 cm indicate active cryoturbation and occur sparsely across many of the sites. Usually the fine-grained terrain is characterised by a continuous cover of cryptogamic crust, lichens (especially *Cladonia nivalis*), and mosses with additional sparse shrubs (particularly *Salix herbacea*), herbs (e.g. *Ranunculus glacialis, Silene acaulis*, and *Saxifraga groenlandica*), and graminoides (*Carex bingelowii, Deschampsia alpina, Festuca ovina, Poa alpina*, and *Luzula spicata*). At a number of sites, especially those on the north-facing slope of Juvflye (Juv 1–12) but also at some with easterly aspect (Juv 13, 19), small solifluction lobes occur in the fine-grained terrain (Fig. 4). These solifluction lobes are commonly 1 - 2 m wide with risers up to 30 cm high and treads about 2 m long. They are often arranged in downslope sequences and can aptly be termed 'solifluction terracettes' (cf. Raczowska, 2009). At a few coarse stripes on the northern slope of Juvflye the sound of subsurface water trickling downslope underneath the surface boulders was

noted, but no surface water was visible during the fieldwork. Without obvious sources like snow patches at the surface, the origin of this subsurface water is likely to have been thawing permafrost resulting in piping and the potential erosion of remaining fines.

4.2. R_{Rock}-values and their interpretation

A total of 9,200 boulders were sampled from sorted stripes on Juvflye. The range of mean R_{Rock}-values is comparatively narrow (51.15 to 55.50) and overlaps with those previously obtained for sorted circles (Tab. 3). Unlike moraines, where the potential for incorporation of pre-exposed boulders or post-depositional disturbance is greater, patterned ground and its diachronous surfaces hardly justify any *a priori* rejection of potential outliers. Furthermore, no consistent patterns could be detected between consecutive downslope subsamples from individual stripes (Fig. 5). Although most sites show an essentially random pattern, a few sites seem to demonstrate a weak increase in mean R_{Rock}-value downslope (e.g. Juv 12; Fig. 5). Thus, all subsequent analyses of R_{Rock}-values are based on data sets of 400 boulders per site.

Visual inspection of histograms prepared for each site reveals platykurtic distributions with broad plateaus, moderate to narrow tails, negative skew and mostly (16 of 23 sites) negative kurtosis. There is an asymmetry towards higher R_{Rock}-values with comparatively long tails at the lower end (Fig. 6). Furthermore, 17 of the 23 sorted stripe sites investigated fail the Kolmogorov-Smirnov test for normality at $\alpha = 0.10$ (Schönwiese 1992, Sachs 1999; 6 sites fail at $\alpha = 0.01$: Juv 6, 7, 13, 14, 18, and 21). Histogram shapes are similar to those presented by Winkler et al. (2016) for sorted circles on Juvflye and contrast with those of synchronous boulder surfaces (e.g. moraines and small rock-slope failures) which usually display symmetrical unimodal distributions (Matthew and Shakesby, 1984; Winkler, 2014; Matthews et al., 2018). Thus, the characteristic distributions of sorted stripe R_{Rock}-values suggest a complex formation and the exposure of individual clasts to subaerial weathering over relatively long periods of time.

Although the range of R_{Rock}-value means for sorted stripe sites on Juvflye is comparatively narrow and 95 % confidence intervals associated with particular sample sites mostly overlap (Tab. 3; Fig. 7), their relationship to various morphological, sedimentological, and topographical parameters was

inspected visually and tested statistically to detect possible causal relationships. As displayed on Fig. 7, there is no apparent relationship between R_{Rock}-value means and site aspect. Linear regression analyses performed on the data sets for morphological parameters of coarse stripes (average stripe width, length, and distance between individual stripes) yield coefficients of determination that confirm no statistically significant relationships (Fig. 8c,d,e). No relationship between mean R_{Rock}-value and clast roundness parameterised as *ir* can be detected (Fig. 8f).

There is no apparent relationship between R_{Rock}-value means and slope angle measured at the sites (Fig. 8b). Contrary to the sorted circles sites on Juvflye, no clear relationship between mean R_{Rock}-value and the altitude of the investigated sorted stripe sites emerges when the complete data set is considered (Fig. 8a). The coefficient of determination (R^2 = 0.027, linear regression analysis, α = 0.05) accordingly does not differ significantly from a random distribution. However, it is important to note that R^2-values increase if the analysis is restricted to those sites with slope gradients below certain thresholds (Tab. 4). The lower the slope gradient of the sorted stripe sites, the stronger the relationship becomes between mean R_{Rock}-value and altitude, and the better the correspondence with the sorted circles data. In summary, there is no significant altitudinal gradient if all sites are included in the analysis and none of the other parameters analysed reveal non-random relationships. Therefore, the variability in R_{Rock}-values derived from the sorted stripe sites is essentially random and remains largely unexplained.

4.3. Control points and Schmidt-hammer exposure-age dating (SHD)

Two nearby sites within the recent glacier foreland of Vesljuvbrean designated as local 'young' control points yield different mean R_{Rock}-values but overlapping confidence intervals (Tab. 5). Site y2 is the preferred choice as the higher mean R_{Rock}-value is likely be more representative of fresh, unweathered boulder surfaces. In addition, the amalgamated data set of both sites from the locality serves as an alternative for the 'young' control point required for calculation of the local SHD-calibration equation. Based on its proximity to the current glacier margin and observations during fieldwork, 2,000 CE is the adopted average date for boulder exposure. The values are close to those of 'young' control points obtained by Winkler & Matthews (2014) from glacially-scoured bedrock

deglaciated around 1,900 CE at Storbrean and Leirbrean, located west of the study area at somewhat lower altitudes. The 'young' control point selected is, therefore, rated as reliable and representative for the sorted stripes.

Although no morphological or lithological peculiarity was noted during fieldwork, one segment (site x1.3) of the moraine sampled as the potential 'old' control point (Fig. 1; see 3.2) yields a slightly different mean than the two other segments that show almost identical mean R_{Rock}-values (Tab. 6). Consequently, for the 'old' control point a data set combining only sites x1.1 and x1.2 was given preference. Nevertheless, use of all three segments serves as an alternative. The difference between results for these moraine boulders and the second 'old' control point on nearby glacially-scoured bedrock (x2 on Fig. 1) is minor, as is the difference to the 'old' control points on bedrock obtained by Winkler & Matthews (2014; Tab. 6). Because boulder surfaces were sampled from both the coarse stripes and the 'young' control point, the moraine is considered as the more representative 'old' control point here. However, the 'old' control point on bedrock is also utilised for the calculation of alternative local SHD-calibration equations (Tab.7). The purpose of this exercise is to obtain an indication of the potential error associated with local SHD-calibration equation calculation resulting from the selection of particular control points.

An opportunity to assess the validity of SHD-calibration equation 'Juvflye 1' as the preferred choice and to review its performance against the alternative options is provided by SHD-ages for sorted circles on Juvflye (Winkler et al. 2016). SHD-ages of the latter were exclusively based on mechanical Schmidt-hammer data and application of the regional Jotunheimen calibration equation of Matthews and Owen (2010). Winkler et al. (2016) additionally obtained RockSchmidt data at three sites of that study that were not considered with any age calculations. Ideally, a reliable local calibration equation for the RockSchmidt should yield identical SHD-ages for the sorted circle sites with these previously published mean R_{Rock}-values. Performance of the preferred and the alternative SHD-calibration equations with these data has been tested accordingly (Tab. 8). Given the potential uncertainties involved, the resulting SHD-ages for 'Juvflye 1' and some alternative equations (e.g. Juvflye '3', 'Juvflye 6') show good agreement. Differences between the individual results of local SHD-calibration equations are relatively small and exhibit overlapping error ranges. Thus, the selection of 'Juvflye 1',

which shows a good fit in addition to being solely based on boulder surface data, appears to be as justified. The 'regional' calibration equation based on data from Winkler and Matthews (2014; see Tabs. 5-7) produces a considerably poorer 'fit' (Tab. 8) so this equation is not considered in subsequent analyses. SHD-ages from application of the preferred local calibration equation 'Juvflye 1' are displayed in Tab. 9. Results for the sorted stripe sites range from 7,975 ± 370 to 6,660 ± 355 years ago and place their stabilisation close to the onset of the HTM (Fig. 9). This range of SHD-ages corresponds well with the supposed stabilisation of sorted circles as reported by Winkler et al. (2016).

The age of the terminal moraine serving as the 'old' control point follows the widely accepted assumption that Juvflye was deglaciated following the Erdalen event ~9.7 kyr ago (see 2.2) and provides comparability with our previous SHD dating of sorted circles. Given the lack of local numerical age constraints, alternative calibration equations derived from the preferred 'Juyflye 1' equation for hypothetical older moraine ages of 10.2 kyr ago (i.e. early Erdalen event; Nesje and Dahl, 1993; Matthews et al., 2008; Matthews and Winkler, 2011), 11.0 kyr ago (i.e. Preboreal Oscillation; Bakke et al. 2005, Nesje 2009), and 11.7 kyr ago (i.e. Younger Dryas; Lohne et al, 2012, 2013; Hughes et al. 2016) have also been calculated (Tab.10a). This was undertaken in light of recent studies on deglaciation patterns close to the study area by Marr et al. (2018, 2019) and previous work in the wider region (Dahl et al. 1997; Lie et al. 2004; Goehring et al. 2008) that points towards a relatively thin Late Glacial and early Holocene Scandinavian Ice Sheet and, hence, the possibility of an earlier deglaciation of the high-altitude plateaus in Jotunheimen. The SHD-ages obtained from these alternative calibration equations are consistently older (Tab.10b) and are a logical consequence of the older ages assigned to their respective 'old' control points. If future research demonstrates that the currently widely accepted age of 9.7 kyr ago for local deglaciation needs to be amended, this will automatically affect all other local SHD-ages in Jotunheimen.

5. Discussion

5.1. Methodological considerations

In the current study, the efficiency of the RockSchmidt with large data sets, as previously highlighted by Winkler et al. (2016) and Winkler and Lambiel (2018), is again convincingly demonstrated. This confirms the RockSchmidt is a good alternative to the mechanical Schmidt-hammer (cf. Winkler and Matthews, 2014). Our study has, furthermore, demonstrated that it is beneficial to retain the recorded R_{Rock}-values obtained on the manufacturer's test anvil during the recommended regular calibration tests (Winkler and Matthews, 2016). Even small offsets of different instruments within the specified calibration window ($R_{Rock} = 91 \pm 2$ for the N-type RockSchmidt; Proceq, 2014) can generate uncertainties with their subsequent implications for comparative SHD-studies if the R_{Rock}-values obtained fall within narrow ranges. For correction of any offset, applying a correction factor based on test anvil data to every individual impact resulting in a proportional correction seems the appropriate procedure. This is for mechanical reasons, because the most likely cause for any deviation of the instrument from its original calibration will be deterioration of the spring as part of its spring-loaded plunger. These procedures should help to minimise possible instrumental bias.

In this study the opportunity was taken to establish a new local SHD-calibration equation specific to the electronic Schmidt-hammer. This avoided the need to apply a conversion of the newly obtained R_{Rock}-values to (mechanical) R-values as introduced by Winkler and Matthews (2014) and to apply existing calibration equations for mechanical Schmidt-hammers such as the 'Jotunheimen' SHD-calibration equation (Matthews and Owen, 2010). But would application of such a conversion have yielded comparable results in our case? The difference between R_{Rock}- and R-value means on the standard test anvil is 8.5 according to Winkler and Matthews (2014) and for sorted circles on Juvflye, Winkler et al. (2016) found corresponding differences. Adopting this value yields, for example, converted mean R-values of 45.45 ± 1.14 for site Juv 8 (mean R_{Rock}-value: 53.95 ± 1.14; Tab. 3) and 42.91 ± 1.15 for site Juv 9 (mean R_{Rock}-value: 51.41 ± 1.15). Application of the 'Jotunheimen' SHD-calibration equation by Matthews and Owen (2010) yields SHD-ages of $7,180 \pm 400$ (Juv 8) and $8,060 \pm 400$ years ago (Juv 9). These results are very similar to those obtained in the current study ($7,160 \pm 370$ (Juv 8) and $7,975 \pm 370$ years ago (Juv 9); Tab. 9). The conclusions of Winkler and Matthews (2014) regarding interconvertibility of data from mechanic and electronic Schmidt-hammers can, therefore, be fully supported.

The shape of the SHD-calibration curve for Juvflye is not considered a potential source of uncertainty for reasons given previously (see 3.3). Although the alternative calibration equations based on different 'young' and 'old' control points (Tab. 7) produce different SHD-ages (Tab. 8), these differences are relatively minor. Selection of the preferred control points cannot, therefore, be regarded as an important source of potential error. The 'young' control point is also not problematic, but the 'known' age assigned to the 'old' control points has not independently been verified by local numerical dates (see 4.3). Thus, our assumed date for deglaciation may require revision in the future with the possibility that the SHD-ages for sorted stripes would become older (Tab. 10). Such a change to SHD-ages would, however, have little influence on the substantive conclusions reached in this paper or on comparative analyses with the other landforms on Juvflye.

5.2 Morphodynamic and palaeoclimatic implications

Sorted stripes constitute diachronous landforms characterised by relatively long histories of development. Winkler et al. (2016) comprehensively discuss interpretative problems of SHD-ages from patterned ground in contrast to exposure ages from synchronous landforms related to singular events. The oldest boulder exposure ages appear to coincide with final deglaciation, and possible inheritance effects from boulders subjected to prior exposure on the surface of the local till sheet appear unimportant. Although some aspects of the detailed mechanics for sorted patterned ground formation have not been fully resolved, upfreezing of coarse clasts previously buried below the surface is certainly one of the main processes to be considered (see Ballantyne, 2018, and references therein). The moment these clasts become exposed to subaerial weathering represents a 'maximum' age for patterned ground formation. Synchronous or subsequent operating processes such as lateral frost sorting, solifluction, and frost creep may result in dislocation and, more importantly, possible tilting or rotation of boulders prior to their final stabilisation (Kääb et al., 2014). Previously unexposed surfaces successively become affected by subaerial weathering and represent a 'minimum' age when the features finally stabilise and any substantial morphodynamic activity ceases (see below).

Mean R_{Rock}-values obtained sequentially along coarse stripes are effectively randomly distributed (Fig. 5). If frost creep processes played a significant role in stripe formation, boulders would predominantly be incorporated at their upslope ends, and a general pattern of lower R_{Rock}-values and increasing exposure ages would be expected downslope, in some ways similar to the situation with rock glaciers (cf. Frauenfelder et al., 2005; Kellerer-Pirklbauer et al., 2008; Rode and Kellerer-Pirklbauer et al., 2011; Scapozza et al., 2014, Winkler and Lambiel, 2018). This is not the case with the coarse stripes investigated. One possible explanation is that boulders become laterally entrained along the full lengths of the coarse stripes rather than at the upslope end. In this context, another unknown factor is to what extent movement by creep or solifluction processes within the coarse stripes cause the boulders to rotate. For ploughing boulders embedded in fine-grained substrate rotation during solifluction has been demonstrated (Ballantyne, 2018). But it is unclear if and how frequently such rotation occurs within coarse stripes. Needle ice, which has been reported to play a role with small-scale sorted stripe formations (Mackay and Mathews, 1974; Werner and Hallet, 1993; Li et al., 2018), would be ineffective in relation to clasts of boulder size within coarse stripes. A reverse pattern of increasing R_{Rock}-values towards the lower sections of the stripes, implying early stabilisation at their upslope end with continuing disturbance of their downslope sections, occurs only rarely. Consistent mean R_{Rock}-values within narrow ranges for entire sorted stripes are also absent. The apparent random variability is, however, comparable to the pattern described for sorted circles by Winkler et al. (2016). One may, therefore, conclude that all processes involved in the formation of sorted stripes on Juvflye acted more-or-less simultaneously – including those that are only effective on terrain with slope gradients too steep for the formation of sorted circles.

Whereas the range of mean R_{Rock}-values and SHD-ages of the sorted stripe sites on Juvflye is, along with the random distribution of R_{Rock}-values within each site, similar to those of sorted circles (Winkler et al., 2016), the lack of a significant altitudinal gradient in relation to the complete data set of sorted stripe sites is remarkable. The reason could be the number of sorted stripe sites investigated (23) compared to sorted circles (5) or involve a causal explanation, or both. Patterned ground data provided by Cook-Talbot (1991) do not show any altitudinal trends and cover multiple other locations in Jotunheimen. However, the strong and statistically significant relationship obtained for sorted circles on Juvflye makes it unlikely that the relationship is an artefact. Furthermore, it seems likely

that there is a logical explanation for the apparent altitudinal gradient that emerges for sorted stripe sites at relatively low slope angles (Tab. 4). This suggests that some individual processes associated with sorted circle formation are overridden on relatively steep slope angles by gelifluction, the process specific to sorted stripes. Rejecting any causal relationship caused by chemical or physical weathering intensity, Winkler et al. (2016) concluded that chronological factors most likely determined the altitudinal gradient in relation to sorted circles. Thus, gelifluction and specific slope-related factors (e.g. drainage conditions) seem to effectively perturb the chronological signal that is evident in relation to the altitudinal gradient in sorted circle stabilisation on flat terrain.

Only very restricted signs of recent disturbance of the sorted stripes were recorded during fieldwork. Combined with the almost completely lichen-covered boulders (Fig. 3), this provides evidence for the relict status and a general lack of postdepositional remobilisation or recent movement of the coarse stripes. These observations agree with previous work by Winkler et al. (2016) and the findings of Donner (2019) regarding small secondary polygonal features (frost crack networks and/or sorting of relatively small clasts) nested within the fine-grained centres of well-developed sorted circles above ~1,850 m a.s.l. Recent post-exposure modification of boulders in coarse stripes can accordingly be rated as negligible and we are in no doubt that the mean boulder exposure age of the coarse stripes simultaneously indicates the timing of (1) the most active upfreezing, and (2) the final stabilisation of boulders.

Limited recent morphodynamic activity of patterned ground on Juvflye as documented by their SHD-ages may, at first sight, appear inconsistent with likely variations in altitudinal limits of permafrost during the Holocene (Lilleøren et al., 2012). Sorted stripe sites above ~1,850 m a.s.l. appear to have been underlain by continuous permafrost even during the HTM. All other sites, now above the postulated current lower limit of alpine permafrost, should have seen late Holocene re-aggradation of permafrost culminating during the LIA. This leads us to the conclusion that since the onset of the HTM coincided with stablisation of the sorted stripes, permafrost is no longer a key factor in the morphodynamics of the patterned ground.

In addition to differential frost heave with various feedback mechanisms (Nicholson, 1976; Mackay, 1984; Kessler et al., 2001; Kessler and Werner, 2003; Peterson and Krantz, 2003), a circulatory

model of intermittent motion of thawed soil in the active layer, better described as buoyancy-induced soil circulation, is widely accepted as an explanation for patterned ground formation (Hallet and Waddington, 1992; Washburn, 1989; Hallet, 1990, 2013). A particular ratio between sorted circle size and depth of the active layer has been suggested (Hallet and Prestrud, 1986; Hallet et al., 1988). With deeper active layers (i.e. convection layers), soil convection and resulting patterned ground formation should be greatly accelerated. Hallet and Prestrud (1986) conclude that maximum efficiency for sorted circle formation still recently active in their study region (Western Spitsbergen) occurred during the regional HTM. In contrast, patterned ground formation evidently terminated during the regional HTM on Juvflye. It may be, however, that a certain (yet undetermined) threshold of active layer depth in relation to feature size exists, above which the depth of the permafrost table it is too great for the circulatory model to work effectively.

The most effective contribution of permafrost to the formation of large-scale sorted patterned ground is considered to be its function as an impermeable aquitard (Ballantyne, 2018). In consequence, the increasing depth of the active layer and subsequent permafrost degradation at lower altitudes due to rising temperature during the HTM may significantly have changed crucial soil moisture conditions such as freezing rates (Vandenberghe, 1988; Luoto and Hjort, 2004) or the moisture gradient (Hallet and Prestrud, 1986) and related thermodynamics (Van Vliet-Lanoë, 1988, 1998; Williams and Smith, 1989). The effect of decreasing soil moisture on patterned ground activity has been highlighted by studies on recently deglaciated glacier forelands in Jotunheimen (Ballantyne and Matthews, 1982; Matthews et al., 1998; Haugland, 2004), which could serve as a modern analogue in this context. Subsequent permafrost aggradation or re-aggradation in the late Holocene was not successful in re-establishing the processes that had ceased processes previously, either because active layer conditions are now sufficiently different to those that operated in the early Holocene or because stabilisation of patterned ground prevented any further development. Ødegård et al. (1988) suggest that a decreasing quantity of fines may no longer have been sufficient to support active frost processes. Exhaustion of boulders from the subsurface of the fine-grained terrain constitutes another possibility for recent inactivity. Finally, with the cessation of aforementioned processes of patterned ground formation on flat terrain, solifluction may remain active, although restricted to the fine grained

soil domain. This agrees with our observations of small solifluction lobes in the fine-grained area between the otherwise inactive coarse stripes (Fig.4).

For the formation of patterned ground on Juvflye, permafrost aggradation must have commenced shortly after deglaciation leaving a time window sufficiently long for the widespread development of these large-scale features (e.g. sorted circles of up to 6 m width) prior to their subsequent stabilisation close to the onset of the HTM. The ~1,500 to 2,000 year time span between deglaciation of Juvflye and patterned ground stabilisation (here presumed synchronous for sorted circles and sorted stripes) is consistent with the model of Kessler et al. (2001) for sorted circle formation. This model predicts that a time period of 750 years is necessary for formation of sorted circles with a width of 3.6 m. Rapid formation of permafrost in rock slopes following deglaciation has recently been demonstrated using models for the fjord region of western Norway (Steiger et al., 2016; Myhra et al., 2017). Although these results cannot simply be transferred to early Holocene Juvflye with its different environmental conditions, rapid permafrost aggradation following deglaciaton seems reasonable (Lilleøren et al., 2012).

6. Conclusions

We conducted measurements with an electronic Schmidt-hammer (RockSchmidt) on 23 selected sites of sorted stripes representing different topographical and morphological settings on Juvflye, developed a local calibration equation specific to the RockSchmidt, applied Schmidt-hammer exposure-age dating (SHD) to sorted stripes for the first time, and discussed the methodological, morphodynamic, and palaeoclimatic implications of our results. The following conclusions can be drawn:

• The RockSchmidt was successfully applied and its efficiency demonstrated. All established procedures introduced for age-calibration and SHD based on the mechanical Schmidt-hammer can be followed without need for adjustment. The previously established interconvertibility of data obtained with mechanical and electronic Schmidt-hammers was confirmed.

• Mean R_{Rock}-values from the sorted stripes showed a narrow range of variability (51.15 to 55.50) and corresponded closely to previous data from sorted circles on Juvflye (51.12 to 55.03). In contrast to the altitudinal gradient in mean R_{Rock}-value and age established previously for sorted circles, a similar relationship was only indicated for sorted stripe sites with low slope gradients (< 9°). No other clear relationship to potential morphological, sedimentological, and topographical parameters affecting R_{Rock}-values was found within the data set.

• Application of a local RockSchmidt SHD-calibration equation revealed that the stabilisation of sorted stripes occurred between 7,976 ± 370 and 6,660 ± 355 years ago around the onset of the regional Holocene Thermal Maximum. These SHD-ages conform to age estimates for stabilisation of the previously investigated sorted circles, demonstrate the relict status of the patterned ground on Juvflye and reflect the lack of any substantial recent morphodynamic activity associated with either the sorted stripes or sorted circles.

• Possible explanations for the early mid-Holocene stabilisation include decreasing soil moisture with its effect on frost activity, linked to insufficient fine-grained substrate for high frost susceptibility, and/or the exhaustion of coarse boulders from centres of frost heave and frost sorting.

• The reasonably well-constrained altitudinal variability of permafrost in Jotunheimen does not align with the timing of the stabilisation of patterned ground on Juvflye. Re-aggradation of permafrost in the late Holocene, which culminated in the 'Little Ice Age', seems to have had no morphodynamic impact on the patterned ground, neither at high-altitude sites presumably underlain by permafrost during the entire Holocene nor at the other sites, currently located above the lower limit of alpine permafrost,

• A remaining source of uncertainty in the SHD-ages is the fixed age assigned to the 'old' control point of the SHD-calibration equation. If ongoing research should show that the age for final deglaciation on Juvflye is older than the currently widely accepted ~9,700 years ago, all SHD-ages from the area will consequently need to be backdated by up to 1,500 years. Comparative analyses with other local periglacial and permafrost features will, however, be unaffected.

Acknowledgements

References

Aa, A.R., Sjåstad, J.A., 2000. Schmidt hammer age evaluation of the moraine sequence in front of Bøyabreen, western Norway. Norsk Geol. Tidsskr. 80 27−32.

Ahlmann, H.W., 1919. Geomorphological studies in Norway. Geogr. Ann. 1, 1−146 + 193−255. https://doi.org/10.2307/519765.

Bakke, J., Dahl, S.O., Nesje, A., 2005. Lateglacial and early Holocene palaeoclimatic reconstruction based on glacier fluctuations and equilibrium-line altitudes at northern Folgefonna, Hardanger, western Norway. J. Quaternary Sci. 20, 179–198. https://doi.org/10.1002/jqs.893.

Ball, D.F., Goodier, R., 1968. Large Sorted Stone-Stripes in the Rhinog Mountains, North Wales. Geogr. Ann. A 50, 54–59. https://doi.org/10.2307/520871.

Ballantyne, C.K., 2001. The sorted stone stripes of Tinto Hill, Scot. Geogr. J. 117,313−324. https://doi.org/10.1080/00369220118737131

Ballantyne, C.K., 2013. Patterned ground. In: Elias, S.A.. Mock, C.J. (Eds.), Encyclopedia of Quaternary Science, 2nd edition, volume 3. Elsevier, Amsterdam, pp. 452–463.

Ballantyne, C.K., 2018. Periglacial geomorphology. Wiley Blackwell, Chichester.

Ballantyne, C.K., Harris, C., 1994. The Periglaciation of Great Britain. University Press, Cambridge.

Ballantyne, C.K. , Matthews, J.A., 1982. The development of sorted circles on recently deglaciated terrain, Jotunheimen, Norway. Arctic Alp. Res. 14, 341–354. https://doi.org/10.1080/00040851.1982.12004316.

Barry, R.G., Gan, T.Y., 2011. The global cryosphere: past, present, future. University Press, Cambridge.

Battey, M.H., Bryhni, I., 1981. Berggrunnen og landskapet. In: Garmo, T.T., Marker, E. (Eds.), Norges nasjonalparker 10 – Jotunheimen. Luther, Oslo, pp. 21–33.

Battey, M.H., McRitchie, W.D., 1973. A geological traverse across the pyroxene-granulites of Jotunheimen in the Norwegian Caledonides. Norsk Geol. Tidsskr. 53, 237–265.

Battey, M.H., McRitchie, W.D., 1975. The petrology of the pyroxene-granulite facies rocks of Jotunheimen, Norway. Norsk Geol. Tidsskr. 55, 1–49.

Beniston, M., Farinotti, D., Stoffel, M., Andreassen, L.M., Coppola, E., Eckert, N., Fantini, A., Giacona, F., Hauck, C., Huss, M., Huwald, H., Lehning, M., López-Moreno, J.I., Magnusson, J., Marty, C., Morán-Tejéda, E., Morin, S., Naaim, M., Provenzale, A., Rabatel, A., Six, D., Stötter, J., Strasser, U., Terzago, S., Vincent, C., 2018. The European mountain cryosphere: a review of its current state, trends, and future challenges. Cryosphere 12, 759–794. https://doi.org/10.5194/tc-12-759-2018.

Böhlert, R., Egli, M., Maisch, M., Brandová, D., Ivy-Ochs, S., Kubik, P.W., Haeberli, W., 2011a. Application of a combination of dating techniques to reconstruct the Lateglacial and early Holocene landscape history of the Albula region (eastern Switzerland). Geomorphology 127, 1–13. https://doi.org/10.1016/j.geomorph.2010.10.034.

Böhlert, R., Compeer, M., Egli, M., Brandová, D., Maisch, M., Kubik, P.W., Haeberli, W., 2011b. A combination of relative-numerical dating methods indicates two high Alpine rock glacier activity phases after the glacier advance of the Younger Dryas. Open Geography J. 4, 115 – 130. https://doi.org/10.2174/1874923201003010115.

Büdel, J., 1981. Klima-Geomorphologie. 2nd edition, Bornträger, Berlin/Stuttgart.

Caine, N., 1974. The geomorphic processes of the alpine environment. In: Ives, J.D. and Barry, R.G. (Eds.), Arctic and Alpine Environments. Methuen, London, pp. 721–748.

Cook-Talbot, J.D., 1991. Sorted circles, relative-age dating and palaeoenvironmental reconstruction in an alpine periglacial environment, eastern Jotunheimen, Norway: lichenometric and weathering-based approaches. Holocene 1, 128–141. https://doi.org/10.1177/095968369100100205.

Corte, A.E., 1963. Particle sorting by repeated freezing and thawing. Science 142, 499–501. https://doi.org/10.1126/science.142.3591.499.

Dahl, S. O., Nesje, A., Øvstedal, J., 1997. Cirque glaciers as morphological evidence for a thin Younger Dryas ice sheet in east-central southern Norway. Boreas 26, 161–180. https://doi.org/10.1111/j.1502-3885.1997.tb00850.x.

Dahl, S.O., Nesje, A., Lie, Ø., Fjordheim, K., Matthews, J.A., 2002. Timing, equilibrium-line altitudes and climatic implications of two early-Holocene glacier glacier readvances during the Erdalen event at Jostedalsbreen, western Norway. Holocene 12, 17–25. https://doi.org/10.1191/0959683602hl516rp.

Donner, A., 2019. Räumliche Verortung periglazialer Reliefformen im Jotunheimen, Norwegen: Ein regionaler Ansatz zur Identifizierung und Analyse bestimmender Einflussfaktoren der natürlichen Rahmenbedingungen. Unpublished M.Sc. thesis, Würzburg, University of Würzburg.

Etzelmüller, B., Romstad. B., Fjellanger, J., 2007. Automatic regional classification of topography in Norway. Norw. J. Geol. 87, 167–180.

Evans, D.J.A., Benn, D.I., 2004. Practical Guide to the Study of Glacial Sediments. London, Arnold.

Evans, D.J.A., Archer, S. and Wilson, D.J.H., 1999. A comparison of the lichenometric and Schmidt hammer dating techniques based on data from the proglacial areas of some Icelandic glaciers. Quaternary Sci. Rev. 18, 13–41. https://doi.org/10.1016/S0277-3791(98)00098-5.

Farbrot, H., Hipp, T.F., Etzelmüller, B., Isaksen, K., Ødegård, R.S., Schuler, T.V., Humlum, O., 2011. Air and ground temperature variations observed along elevation and continentality gradients in southern Norway. Permafrost Periglac. 22, 343–360. https://doi.org/10.1002/ppp.733.

Fossen, H., Pedersen R.-B., Bergh. S., Andresen, A., 2008. Creation of a mountain chain. The building up of the Caledonides, about 500-405 Ma. In: Ramberg, I., Bryhni, I., Nøttvedt, A., Rangnes, K. (Eds.), The making of a land – Geology of Norway. NGF, Trondheim, pp.178–231.

Francou, B., Le Méhauté, N., Jomelli, V., 2001. Factors Controlling Spacing Distances of Sorted Stripes in a Low-Latitude, Alpine Environment (Cordillera Real, 16 °S, Bolivia). Permafrost Periglac. 12, 367–377. https://doi.org/10.1002/ppp.398.

Frauenfelder, R., Laustela, R., Kääb, A., 2005. Relative age-dating of Alpine rock glaciers. Z. Geomorphol. 49, 145–166. https://doi.org/0372-8854/05/0145.

French, H.M., 1988. Active layer processes. In: Clark, M.J. (Ed.), Advances in periglacial geomorphology. Chichester, Wiley, pp.151–177.

French, H.M., 2018. The Periglacial Environment, 4th edition. Wiley, Chichester.

Gisnås, K., Etzelmüller, B., Farbrot, H., Schuler, T.V., Westermann, S., 2013. CryoGRID 1.0: Permafrost Distribution in Norway estimated by a Spatial Numerical Model. Permafrost Periglac. 24, 2 – 19. https://doi.org/10.1002/ppp.1765.

Gisnås, K., Etzelmüller, B., Lussana, C., Hjort, J., Sannel, B.K., Isaksen, K., Westermann, S., Kuhry, P., Christiansen, H.H., Frampton, A., Åkerman, J., 2017. Permafrost Map for Norway, Sweden and Finland. Permafrost Periglac. 28, 359–378. https://doi.org/10.1002/ppp.1922.

Gjessing, J., 1967. Norway´s paleic surface. Norsk Geogr. Tidsskr. 21, 69−132. https://doi.org//10.1080/00291956708621854.

Gjessing, J., 1978. Norges landformer. Universitetsforlaget, Oslo/Bergen/Tromsø.

Goehring, B. M., Brook, E. J., Linge, H., Raisbeck, G. M., Yiou, F., 2008. Beryllium-10 exposure ages of erratic boulders in Southern Norway and implications for the history of the Fennoscandian Ice Sheet. Quaternary Sci. Rev. 27, 320–336. https://doi.org/10.1016/j.quascirev.2007.11.004.

Goldthwait, R.P., 1976. Frost-sorted patterned ground: a review. Quaternary Res. 6, 27−35. https://doi.org/10.1016/0033-5894(76)90038-7.

Goudie, A.S., 2006. The Schmidt Hammer in geomorphological research. Prog. Phys. Geogr. 30, 703–718. https://doi.org/10.1177/0309133306071954.

Hall, K., 1983. Sorted stripes on sub-Antarctic Kerguelen Island. Earth Surface Processes and Landforms 8, 115 – 124. https://doi.org/10.1002/esp.3290080203.

Hallet, B., 1990. Self-organization in freezing soils – from microscopic ice lenses to patterned ground. Can. J. Phys. 68, 842–852. https://doi.org/10.1139/p90-122.

Hallet, B., 2013. Stone circles: form and soil kinematics. Philos. T. R. Soc. A 371, 20120357. https://doi.org/10.1098/rsta.2012.0357.

Hallet, B., Prestrud, S., 1986. Dynamics of periglacial sorted circle in western Spitsbergen. Quaternary Res. 26, 81–99. https://doi.org/10.1016/0033-5894(86)90085-2.

Hallet, B., Waddington, E.D., 1992. Buoyancy forces induced by freeze-thaw in the active layer: implications for diapirism and soil circulation. In: Dixon, J.C. and Abrahams, A.D. (Eds.), Periglacial geomorphology. Wiley, Chichester, pp.305 - 325.

Hallet, B., Prestrud Andersen, S., Stubbs, C.W., Carrington Gregory, C. 1988. Surface soil displacements in sorted circles, western Spitsbergen. In: Senneset, K. (Ed.), 5th International conference on permafrost proceedings vol.1. Tapir, Trondheim, pp. 770 – 775.

Harris, C., Arenson, L.U., Christiansen, H.H., Etzelmüller, B., Frauenfelder, R., Gruber, S., Haeberli, W., Hauck, C., Hoelzle, M., Humlum, O., Isaksen, K., Kääb, A., Kern-Luetschg, M.A., Lehning, M., Matsuoka, N., Murton, J.B., Noezli, J., Phillips, M., Ross, N., Seppälä, M., Springman, S.M. and Vonder Mühll, D.V., 2009. Permafrost and climate in Europe: monitoring and modelling thermal, geomorphological and geotechnical responses. Earth Sci. Rev. 92, 117-171. https://doi.org/10.1016/j.earscirev.2008.12.002.

Harris, S.A., 1988. The alpine periglacial zone. In: Clark, M.J. (Ed.), Advances in Periglacial Geomorphology. Chichester, Wiley, pp. 369–413.

Hauck, C., Isaksen, K., Vonder Mühll, D., Sollid, J.L., 2004. Geophysical surveys designed to delineate the altitudinal limit of mountain permafrost: an example from Jotunheimen, Norway. Permafrost Periglac. 15, 191–205. https://doi.org/10.1002/ppp.493.

Haugland, J.E., 2004. Formation of patterned ground and fine-scale soil development within two late Holocene glacial chronosequences: Jotunheimen, Norway. Geomorphology 61, 287- 301. https://doi.org/10.1016/j.geomorph.2004.01.004.

Hipp, T., Etzelmüller, B., Farbrot, H., Schuler, T.V., Westermann, S., 2012. Modelling borehole temperatures in Southern Norway – insights into permafrost dynamics during the 20th and 21st century. Cryosphere 6, 553 – 571. https://doi.org/10.5194/tc-6-553-2012.

Hughes, A.L.C., Gyllencreutz, R., Lohne, Ø.S., Mangerud, J., Svendsen, J.I., 2016. The last Eurasian ice sheets – a chronological database and time-slice reconstruction, DATED-1. Boreas 45, 1–45. https://doi.org/10.1111/bor.12142.

Isaksen, K., Holmlund, P., Sollid, J.L., Harris, C., 2001. Three Deep Alpine-Permafrost Boreholes in Svalbard and Scandinavia. Permafrost Periglac. 12, 13-25. https://doi.org/10.1002/ppp 380.

Isaksen, K., Hauck, C., Gudevang, E., Ødegård, R.S., Sollid, J.L., 2002. Mountain permafrost distribution in Dovrefjell and Jotunheimen, southern Norway, based on BTS and DC resistivity tomography data. Norsk Geogr. Tidsskr. 56, 122–136. https://doi.org/10.1080/002919502760056459.

Isaksen, K., Sollid, J.L., Holmlund, P., Harris, C., 2007. Recent warming of mountain permafrost in Svalbard and Scandinavia. J. Geophys. Res. 112, F92S04. https://doi.org/10.1029/2006JF000522.

Isaksen, K., Ødegård, R.S., Etzelmüller, B., Hilbich, C., Hauck, C., Farbrot, H., Eiken, T., Hagen, J.O., Hipp, T.F., 2011. Degrading mountain permafrost in Southern Norway: Spatial and temporal variability of ground temperatures, 1999 – 2009. Permafrost Periglac. 22, 361–377. https://doi.org/10.1002/ppp.728.

Kääb, A., Girod, L., Berthling, I., 2014. Surface kinematics of periglacial sorted circles using structure-from-motion technology. Cryosphere 8, 1041–1056. https://doi.org/10.5194/tc-8-1041-2014.

Kade, A., Romanovsky, V.E,, Walker, D.A., 2006, The N-Factor of Nonsorted Circles Along a Climate Gradient in Arctic Alaska. Permafrost Periglac. 17, 279–289. https://doi.org/10.1002/ppp.563.

Kellerer-Pirklbauer, A., Wangensteen, B., Farbrot, H. and Etzelmüller, B., 2008. Relative surface age-dating of rock glacier systems near Hólar in Hjaltadalur, Northern Iceland. J. Quaternary Sci. 23, 137–151. https://doi.org/10.1002/jqs.1117.

Kessler, M.A., Werner, T.B. 2003. Self-organization of sorted patterned ground. Science 299, 380 – 383. https://doi.org/10.1126/science.299.5605.380.

Kessler, M.A., Murray, A.B., Werner, T.B., Hallet, B., 2001. A model for sorted circles as self-organized patterns. J. Geophys. Res. Sol-EA. 106, 13287–13306. https://doi.org/10.1029/2001JB000279.

Klapyta, P., 2013. Application of Schmidt hammer relative age dating to Late Pleistocene moraines and rock glaciers in the Western Tatra Mountains, Slovakia. Catena 111, 104–121. https://doi.org/10.1016/j.catena.2013.07.004.

Li, A., Matsuoka, N., Niu, F., 2018. Frost sorting on slopes by needle ice: A laboratory simulation on the effect of slope gradient. Earth Surf. Proc. Land. 43,685–694. https://doi.org/10.1002/esp.4276.

Lidmar-Bergström, K., Ollier, C.D., Sulebak, J.R., 2000. Landforms and uplift history of southern Norway. Global Planet Change 24, 211–231. https://doi.org/10.1016/S0921-8181(00)00009-6.

Lie, Ø., Dahl, S.O., Nesje, A., Matthews, J.A., Sandvold, S., 2004. Holocene fluctuations of a polythermal glacier in high-alpine eastern Jotunheimen, central-southern Norway. Quaternary Sci. Rev. 23, 1925–1945. https://doi.org/10.1016/j.quascirev.2004.03.012.

Lilleøren, K., Etzelmüller, B., Schuler, T.V., Gisnås, K., Humlum, O., 2012. The relative age of mountain permafrost – estimation of Holocene permafrost limits in Norway. Global Planet Change 92–93, 209–223. https://doi.org/10.1016/j.gloplacha.2012.05.016.

Lohne, Ø..S.., Mangerund, J., Svendsen, J.I., 2012. Timing of the Younger Dryas glacial maximum in Western Norway. J. Quaternary Sci. 27, 81 – 88. https://doi.org/10.1016/j.quascirev.2007.04.008, 2007.

Lohne, Ø. S., Mangerud, J., Birks, H. H., 2013. Precise ^{14}C ages of the Vedde and Saksunarvatn ashes and the Younger Dryas boundaries from western Norway and their comparison with the Greenland Ice Core (GICC05) chronology, J. Quaternary Sci. 28, 490–500. https://doi.org/10.1002/jqs.2640.

Lukas, S.. Benn, D.I., Boston, C.M., Brook, M., Coray, S., Evans, D.J.A., Graf, A., Kellerer-Pirklbauer, A., Kirkbride, M.P., Krabbendam, M., Lovell, H., Machiedo, M., Mills, S.C., Nye, K., Reinardy, B.T.J., Ross, F.H., Signer, M., 2013. Clast shape and clast transport paths in glacial environments: a critical review of methods and the role of lithology. Earth Sci. Rev. 121, 96–116. https://doi.org/10.1016/j.earscirev.2013.02.005.

Luoto, M., Hjort, J., 2004. Generalized linear modeling in periglacial studies: Terrain parameters and patterned ground. Permafrost Periglac. 15, 327–338. https://doi.org/10.1002/ppp.482.

Lutro, O., Tveten, E., 1996. Geologisk kart over Norge, berggrunnskart Årdal M 1:250.000 Årdal. Trondheim, Norges Geologiske Undersøkelse.

Mackay, J.R., 1984. The frost heave of stones in the active layer above permafrost with downward and upward freezing. Arctic Alp. Res. 16, 439–446. https://doi.org/10.1080/00040851.1984.12004435.

Mackay, J.R., Mathews, W.H., 1974. Movements of sorted stripes, the Cinder Cone, Garibaldi Park, B.C., Canada. Arctic Alp. Res. 6, 347–359. https://doi.org/10.1080/00040851.1974.12003794.

Mangerud, J., Gyllencreutz, R., Lohne, Ø., Svendsen, J.I., 2011. Glacial history of Norway. In: Ehlers, J., Gibbard, P.L., Hughes, P.D. (Eds). Quaternary glaciations – extent and chronology. Elsevier, Amsterdam, pp. 279–298.

Marr, P., Winkler, S., Löffler, J., 2018. Investigations on blockfields and related landforms at Blåhø (Southern Norway) using Schmidt-hammer exposure-age dating: palaeoclimatic and

morphodynamic implications, Geogr. Ann. A. 100, 285–306.

https://doi.org/10.1080/04353676.2018.1474350.

Marr, P., Winkler, S., Binnie, S.A., Löffler, J., 2019. 10Be based exploration of the timing of

deglaciation in two selected areas of southern Norway. E&G Quaternary Sci. J. 68, 165–176.

https://doi.org/10.5194/egqsj-68-165-2019.

Matsuoka, N., 2011. Climate and material controls on periglacial soil processes: Toward improving

periglacial climate indicators. Quat. Res. 75, 356–365. https://doi.org/10.1016/j.yqres.2010.12.014.

Matsuoka, N., Abe, M., Ijiri, M., 2003. Differential frost heave and sorted patterned ground: field

measurements and a laboratory experiment. Geomorphology 52, 73–85.

https://doi.org/10.1016/S0169-555X(02)00249-0.

Matthews, J..A., 1987. Regional variation in the composition of Neoglacial end moraines,

Jotunheimen, Norway: an altitudinal gradient in clast roundness and its possible palaeoclimatic

significance. Boreas 16, 173–188. https://doi.org/ /10.1111/j.1502-3885.1987.tb00769.x.

Matthews, J.A., Dresser, P.Q., 2008. Holocene glacier variation chronology of the

Smørstabbtindan massif, Jotunheimen, southern Norway, and the recognition of century- to

millennial-scale European Neoglacial events. Holocene 18, 181–201.

https://doi.org/10.1177/0959683607085608.

Matthews, J.A., McEwen, L.J., 2013. High-precision Schmidt-hammer exposure-age dating of flood

berms, Vetlestølsdalen, alpine southern Norway: first application and some methodological issues.

Geogr. Ann. A 95, 185–195. https://doi.org/10.1111/geoa.12009.

Matthews, J.A., Owen, G., 2010. Schmidt hammer exposure-age dating: development linear age-

calibration curves using Holocene bedrock surfaces from the Jotunheimen-Jostedalsbreen regions

of southern Norway. Boreas 39, 105–115. https://doi.org/10.1111/j.1502-3885.2009.00107.x.

Matthews, J.A., Shakesby, R.A., 1984. The status of the 'LIttle Ice Age' in southern Norway: a

relative-age dating of Neoglacial moraines with Schmidt hammer and lichenometry. Boreas 13,

333–346. https://doi.org/10.1111/j.1502-3885.1984.tb01128.x.

Matthews, J.A., Wilson, P., 2015. Improved Schmidt-hammer exposure ages for active and relict pronival ramparts in southern Norway, and their palaeoenvironmental implications. Geomorphology 246, 7–21. https://doi.org/10.1016/j.geomorph.2015.06.002.

Matthews, J.A., Winkler, S., 2011. Schmidt-hammer exposure-age dating (SHD): application to early-Holocene moraines and a reappraisal of the reliability of terrestrial cosmogenic-nuclide dating (TCND) at Austanbotnbreen, Jotunheimen, Norway. Boreas 40, 256–270. https:// 10.1111/j.1502-3885.2010.00178.x.

Matthews, J.A., Shakesby, R.A., Berrisford, M.S. and McEwen, L.J., 1998: Periglacial patterned ground on the Styggedalsbreen glacier foreland, Jotunheimen, southern Norway: micro-topographic, paraglacial and geoecological controls. Permafrost Periglac. 9, 147–166. https://doi.org/10.1002/(SICI)1099-1530(199804/06)9:2<147::AID-PPP278>3.0.CO;2-9.

Matthews, J.A., Shakesby, R.A., Schnabel, C., Freeman, S., 2008. Cosmogenic ^{10}Be and ^{26}Al ages of Holocene moraines in southern Norway I: testing the method and confirmation of the date of the Erdalen event (c. 10 ka) at its type-site. Holocene 18, 1155–1164. https://doi.org/10.1177/0959683608096585.

Matthews, J.A., Shakesby, R.A., Owen, G., Vater, A.E., 2011. Pronival rampart formation in relation to snow-avalanche activity and Schmidt-hammer exposure-age dating (SHD): three case studies from southern Norway. Geomorphology 130, 280–288. https://doi.org/10.1016/j.geomorph.2011.04.010.

Matthews, J.A., Nesje, A., Linge, H., 2013. Relict talus-foot rock glaciers at Øyberget, Upper Ottadalen, Southern Norway: Schmidt hammer exposure ages and palaeoenvironmental implications. Permafrost Periglac. 24, 336–346. https://doi.org/10.1002/ppp.1794.

Matthews, J.A., Winkler, S., Wilson, P., 2014. Age and origin of ice-cored moraines in Jotunheimen and Breheimen, Southern Norway: Insights from Schmidt-hammer exposure-age dating. Geogr. Ann. A 96, 531–548. https://doi.org/10.1111/geoa.12046.

Matthews, J.A., McEwen, L., Owen, G., 2015. Schmidt-hammer exposure-age dating (SHD) of snow-avalanche impact ramparts in southern Norway: approaches, results and implications for

landform age, dynamics and development. Earth Surf. Proc. Land. 40, 1705–1718. https://doi.org/ 10.1002/esp.3746.

Matthews, J.A., Owen, G., Winkler, S., Vater, A.E., Wilson, P., Mourne, R.W., Hill, J.L., 2016. A rock-surface microweathering index from Schmidt hammer R-values and its preliminary application to some common rock types in southern Norway. Catena 143, 35–44. https://doi.org/10.1016/j.catena.2016.03.018.

Matthews, J.A., Wilson, P., Mourne, R.W., 2017. Landform transitions from pronival ramparts to moraines and rock glaciers: a case study from the Smørbotn cirque, Romsdalsalpane, southern Norway. Geogr. Ann. A 99, 15 – 37. https://doi.org/10.1080/04353676.2016.1256582.

Matthews, J.A., Winkler, S., Wilson, P., Tomkins, M., Dortch, J., Mourne, R., Hill, J., Owen, G., Tomkins, J., Vater, A., 2018. Small rock-slope failures conditions by Holocene permafrost degradation: a new approach and conceptual model based on Schmidt-hammer exposure-age dating in Jotunheimen, southern Norway. Boreas 47, 1144–1169. https://doi.org/10.1111/bor.12336.

Matthews, J.A., Wilson, P., Winkler, S., Mourne, R., Hill, J., Owen, G., Hiemstra, J.F., Hallang, H., Geary, A.P., 2019. Age and development of active cryoplanation terraces in the alpine permafrost zone at Svartkampan, Jotunheimen, southern Norway. Quaternary Res. 92, 641–664. https;//doi.org/10.1017/qua.2019.41.

McCarroll, D., 1989. Potential and limitations of the Schmidt hammer for relative-age dating: field tests on Neoglacial moraines, Jotunheimen, southern Norway. Arctic Alp. Res. 21, 268–275. https://doi.org/10.1080/00040851.1989.12002738.

McCarroll, D., 1994. The Schmidt hammer as a measure of degree of rock surface weathering and terrain age. In: Beck, C. (Ed.), Dating in Exposed and Surface Contexts. University of New Mexico Press, Albuquerque, pp. 29–45.

Myhra, K.S., Westermann, S., Etzelmüller, B., 2017. Modelled distribution and temporal evolution of permafrost in steep rock walls along a latitudinal transect in Norway by CryoGrid 2D. Permafrost Periglac. 28, 172–182. https//doi.org/ 10.1002/ppp.1884.

Nesje, A., 2009. Late Pleistocene and Holocene alpine glacier fluctuation in Scandinavia. Quaternary Sci. Rev. 28, 2119–2136. https://doi.org/10.1016/j.quascirev.2008.12.016.

Nesje, A., Dahl, S.O., 1993. Lateglacial and Holocene glacier fluctuations and climate variations in western Norway: a review. Quaternary Sci. Rev. 12, 255-261. https://doi.org/10.1016/0277-3791(93)90081-V.

Nesje, A., Whillans, I.M., 1994. Erosion of Sognefjord, Norway. Geomorphology 9, 33–45. https://doi.org/10.1016/0169-555X(94)90029-9.

Nesje, A., Blikra, L.H., Anda, E., 1994a. Dating rockfall-avalanche deposits from the degree of rock-surface weathering by Schmidt hammer tests: a study from Norangsdalen, Sunnmøre, Norway. Norsk Geol. Tidsskr. 74, 108–113.

Nesje, A., McCarroll, D., Dahl, S.O., 1994b. Degree of rock surface weathering as an indicator of ice-sheet thickness along an east-west transect across southern Norway. J. Quaternary Sci. 9, 337–347. https://doi.org/10.1002/jqs.3390090404.

Nicholson, F.H., 1976, Patterned ground formation and description as suggested by low arctic and subarctic examples. Arctic Alp. 8, 329–342. https://doi.org/10.1080/00040851.1976.12003883.

Ødegård, R.S., Sollid, J.L., Liestøl, O., 1987. Juvflya – Kvartærgeologi og geomorfologi M 1:10.000. Geografisk Institutt, Universitetet I Oslo, Oslo.

Ødegård, R.S., Sollid, J.L., Liestøl, O., 1988. Periglacial forms related to terrain parameters in Jotunheimen, southern Norway. In: Senneset, K. (Ed.), 5th International conference on permafrost proceedings vol.3. Tapir, Trondheim, pp. 59–61.

Ødegård, R.S., Sollid, J.L., Liestøl, O., 1992. Ground temperature measurements in mountain permafrost, Jotunheimen, southern Norway. Permafrost Periglac. 3, 231–234. https://doi.org/10.1002/ppp.3430030310.

Ødegård, R.S., Hoelzle, M., Johansen, K.V., Sollid, J.L., 1996. Permafrost mapping and prospecting in southern Norway. Norsk Geogr. Tidsskr, 50, 41–53. https://doi.org/10.1080/00291959608552351.

Ødegård, R.S., Isaksen, K., Mastervik, M., Billdal, L., Engler, M., Sollid, J.L., 1999. Comparison of BTS and Landsat TM data from Jotunheimen, southern Norway. Norsk Geogr. Tidsskr. 53, 226–233. https://doi.org/10.1080/002919599420811.

Patton, H., Hubbard, A., Andreassen, K., Winsborrow, M., Stroeven, A.P., 2016. The build-up, configuration, and dynamical sensitivity of the Eurasian ice-sheet complex to Late Weichselian climatic and oceanic forcing. Quaternary Sci. Rev. 153, 97–121. https://doi.org/10.1016/j.quascirev.2016.10.009.

Patton, H., Hubbard, A., Andreassen, K., Auriac, A., Whitehouse, P.L., Stroeven, A.P., Shackleton, C., Winsborrow, M., Heyman, J., Hall, A.M., 2017. Deglaciation of the Eurasian ice sheet complex. Quaternary Sci. Rev. 169, 148–172. https://doi.org/10.1016/j.quascirev.2017.05.019.

Peterson, R.A., Krantz, W.B., 2003. A mechanism for differential frost heave and its implications for patterned-ground formation. J. Glaciol. 49, 69–80. https://doi.org/10.3189/172756503781830854.

Poole, R.W. & Farmer, I.W. (1980): Consistency and repeatability of Schmidt hammer rebound data during field testing. Consistency and repeatability of Schmidt hammer rebound data during field testing. Int. J. Rock Mech. Min. Sci. Geomech. Abstr. 17, 167–171. https://doi.org/10.1016/0148-9062(80)91363-7.

Powers, M.S., 1953. A new roundness scale for sedimentary particles. Journal of Sedimentary Petrology, 23, 117–119. https://doi.org./10.1306/D4269567-2B26-11D7-8648000102C1865D.

Proceq. 2014. Operating instructions RockSchmidt & Rocklink. Proceq SA, Schwerzenbach.

Raczkowska, Z., 2009. Differentiation of present-day periglacial relief in the high mountains of Europe. Rom. Journ. Geogr. 53, 107–118.

Reusch, H., 1901. Nogle bidrag till forstaaelsen af hvorledes Norges dale og fjelde er blevne til. Norg. Geol. Unders. 32 (Aarbog 1900), 124–263.

Rode, M., Kellerer-Pirklbauer, A., 2011. Schmidt-hammer exposure-age dating (SHD) of rock glaciers in the Schöderkogel-Eisenhut area, Schladminger Tauern Range, Austria. Holocene 22, 761–771. https://doi.org/10.1177/0959683611430410.

Sachs, L., 1999. Angewandte Statistik. 9th edition, Berlin, Springer.

Scapozza, C., Lambiel, C., Bozzini, C., Mari, S., Condera, M., 2014. Assessing the rock Glacier kinematics on three different time scales: a case study from the southern Swiss Alps. Earth Surf. Proc. Land. 39, 2056–2069. https://doi.org/10.1002/esp.3599.

Schönwiese, C-D., 1992. Praktische Statistik für Meteorologen und Geowissenschaftler, 2nd edition. Berlin/Stuttgart, Bornträger.

Shakesby, R.A., Matthews, J.A., Owen, G., 2006. The Schmidt hammer as a relative-age dating tool and its potential for calibrated-age dating in Holocene glaciated environments. Quaternary Sci. Rev. 25, 2846–2867. https://doi.org/10.1016/j.quascirev.2006.07.011.

Shakesby, R.A., Matthews, J.A., Karlén, W., Los, S.O., 2011. The Schmidt hammer as a Holocene calibrated-age dating technique: testing the form of the R-value-age relationship and defining the predicted-age errors. Holocene 21, 615–628. https://doi.org/10.1177/0959683610391322.

Sigmond, E.M.O., Gustavson, M., Roberts, D., 1984. Berggrunnskart over Norge 1:1 milion. Norges Geologiske Undersøkelse, Trondheim.

Slaymaker, O., Embleton-Hamann, C., 2009. Mountains. In: Slaymaker, O., Spencer, T., Embleton-Hamann, C. (Eds.), Geomorphology and Global Environmental Change. Cambridge, University Press, pp. 37 – 70.

Slaymaker, O., Embleton-Hamann, C., 2018. Advances in global mountain geomorphology. Geomorphology 308, 230 – 264. https:/doi.org/10.1016/j.geomorph.2018.02.016.

Steiger, C., Etzelmüller, B., Westermann, S., Myhra, K.S., 2016. Modelling the permafrost distribution in steep rock walls in Norway. Norw. J. Geol. 96, 1–13. https://doi.org/0.17850/njg96-4-04.

Stroeven, A.P., Hättestrand, C., Kleman, J., Heyman, J., Fabel, D., Fredin, O., Goodfellow, B.W., Harbor, J.M., Jansen, J.D., Olsen, L., Caffee, M.W., Fink, D., Lundqvist, J., Rosqvist, G.C., Strömberg, B., Jansson, K.N., 2016. Deglaciation of Fennoscandia. Quaternary Sci. Rev. 147, 91–121. https://doi.org/10.1016/j.quascirev.2015.09.016.

Thompson, W.F., 1990. Climate related landscapes in world mountains: criteria and maps. Z. Geomorphol. Suppl. 78, Bornträger, Stuttgart/Berlin.

Tomkins. M.D., Dortch, J.M., Hughes, P.D., 2016. Schmidt hammer exposure dating (SHED), establishment and implications for the retreat of the last British Ice. Quat. Geochronol. 33, 46–60. https://doi.org/10.1016/j.quageo.2016.02.002.

Tomkins, M. D., Dortch, J. M., Hughes, P. D., Huck, J. J., Stimson, A.G., Delmas, M., Calvet, M., Pallàs, R., 2018a. Schmidt hammer exposure dating (SHED): rapid age assessment of glacial landforms in the Pyrenees. Quaternary Res. 90, 26–37. https://doi.org/10.1017/qua.2018.12

Tomkins, M.D., Hucka, J.J., Dortch, J.M., Hughes, P.B., Kirbride, M.P., Barr, I.D., 2018b. Schmidt Hammer exposure dating (SHED): Calibration procedures, new exposure age data and an online calculator. Quat. Geochronol. 44, 55–62. https://doi.org/10.1016/j.quageo.2017.12.003.

Tucker, M., 1988. Techniques in Sedimentology. Blackwell, London.

Vandenberghe, J., 1988. Cryoturbations. In: Clark, M.J. (Ed.), Advances in Periglacial Geomorphology. Wiley, Chichester, pp.179–198.

Van Vliet-Lanoë, B., 1988. The genesis of cryoturbations and their significance in environmental reconstruction. J. Quaternary Sci. 3, 85–96. https://doi.org/10.1002/jqs.3390030110.

Van Vliet-Lanoë, B., 1991. Different frost heave, load casting and convection: converging mechanisms; a discussion of the origin of cryoturbations. Permafrost Periglac. 2, 123–139. https://doi.org/10.1002/ppp.3430020207.

Van Vliet-Lanoë, B., 1998. Frost and soils: implications for paleosols, paleoclimates and stratigraphy. Catena 34, 157–183. https://doi.org/10.1016/S0341-8162(98)00087-3.

Warburton, J., 2013. Patterned ground and polygons. In: Giordano, J.R., Harbour, J.M. (Eds.), Treatise on Geomorphology, Volume 8 Glacial and Periglacial Geomorphology. Elsevier, Amsterdam, pp.298–312.

Washburn, A.L., 1956. Classification of patterned ground and review of suggested origins. Geol. Soc. Am. Bull. 67, 823–865. https://doi.org/10.1130/0016-7606(1956)67[823:COPGAR]2.0.CO;2

Washburn, A.L., 1979. Geocryology, 2nd edition. Arnold, London.

Washburn, A.L., 1989. Near-surface soil displacement in sorted circles, Resolute area, Cornwallis Island, Canadian High Arctic. Can. J. Earth Sci. 26, 941–955. https://doi.org/10.1139/e89-076.

Werner, B.T., Hallet, B., 1993. Numerical simulation of selforganized stone stripes. Nature 361, 142 – 145. https://doi.org/10.1038/361142a0.

Williams, P.J., Smith, M.W., 1989. The frozen earth. University Press, Cambridge.

Wilson, P., Matthews, J.A., Mourne, R.W., 2017. Relict Blockstreams at Insteheia, Valldalen-Tafjorden, Southern Norway: Their Nature and Schmidt Hammer Exposure Age. Permafrost Periglac. 28, 286–297. https://doi.org/10.1002/ppp.1915.

Wilson, P., Linge, H., Matthews, J.A., Mourne, R.W., Olsen, J., 2019. Comparative numerical surface exposure-age dating (Schmidt hammer and [10]Be) of an early-Holocene rock avalanche at Alstadfjellet, Valldalen, in southern Norway. Geogr. Ann. A 101, 293– 309. https://doi.org/10.1080/04353676.2019.1644815.

Winkler, S., 2005. The 'Schmidt hammer' as a relative-age dating technique: potential and limitations of its application on Holocene moraines in Mt Cook National Park, Southern Alps, New Zealand. New Zeal. J. Geol. Geop. 48, 105–116. https://doi.org/0028–8306/05/4801–0105.

Winkler, S., 2009. First attempt to combine terrestrial cosmogenic nuclide (10Be) and Schmidt hammer relative-age dating: Strauchon Glacier, Southern Alps, New Zealand. Cent. Eur. J. Geosci. 1, 274–290. https://doi.org/10.2478/v10085-009-0026-3.

Winkler, S., 2014. Investigation of late-Holocene moraines in the western Southern Alps, New Zealand, applying Schmidt-hammer exposure-age dating (SHD). Holocene 24, 48–66. https://doi.org/10.1177/0959683613512169.

Winkler, S., Lambiel,, C., 2018. Age constraints of rock glaciers in the Southern Alps/New Zealand – exploring their palaeoclimatic potential. Holocene 28, 778–790. https://doi.org/10.1177/0959683618756802.

Winkler, S., Matthews, J.A., 2014. Comparison of electronic and mechanical Schmidt hammers in the context of exposure-age dating: Are Q- and R-values interconvertible? Earth Surf. Proc. Land. 39, 1128–1136. https://doi.org/10.1002/esp.3584

Winkler, S., Matthews, J.A., 2016. Inappropriate instrument calibration for Schmidt-hammer exposure-age dating (SHD) - A comment on Dortch et al., Quaternary Geochronology 35 (2016), 67- 68, Quat. Geochronol. 36, 102–103. https://doi.org/10.1016/j.quageo.2016.08.009.

Winkler, S., Matthews, J.A., Mourne, R.W., Wilson, P., 2016. Schmidt-hammer exposure ages from periglacial patterned ground (sorted circles) in Jotunheimen, Norway, and their interpretative problems. Geogr. Ann. A 98, 265–285. https://doi.org/10.1111/geoa.12134.

Winkler, S., Donner, A. & Tintrup gen. Suntrup, A., 2020. Periglacial landforms in Jotunheimen, central southern Norway, and their altitudinal distribution. In: Beylich, A.A. (Eds.), Landscapes and Landforms of Norway. Springer, Cham, (in press).

www.met.no – open portal of Meteorologisk insitutt/www.met.no (last accessed 12.09.2019).

www.norgeibilder.no – open portal of Kartverket/www.kartverket.no (last accessed 12.09.2019)

www.senorge.no – open portal in collaboration between Norges Vassdrags- og Energidirektoratet/www.nve.no, Meteorologisk institutt/www.met.no, and Kartverket/www.kartverket.no (last accessed 12.09.2019).

Table 1

Mean air temperature	Jan (°C)	Feb	Mar	Apr	May	Jun	Jul	Aug	Sep	Oct	Nov	Dec
Maximum	-7.2	-5.6	-5.4	-2.1	4.1	4.8	9.6	8.5	4.3	0.2	-1.4	-5.1
Minimum	-12.3	-14.2	-13.3	-9.0	-4.8	-0.3	3.1	2.8	-1.7	-7.3	-12.1	-13.9
Mean	-9.9	-9.8	-9.1	-5.4	-1.5	2.2	5.6	4.3	1.0	-3.1	-6.6	-8.9

Table 2

Site	Altitude (m a.s.l.)	Aspect	Slope angle (°)	Coarse stripe width (m)	Coarse stripe length (m)	Spacing between stripes (m)	IR[1] / dominant clast roundness class
Juv 1	1,820	NW	14	2.0	50	3.5	2.38 / subangular
Juv 2	1,830	N	10	0.9	28	3.4	1.68 / angular
Juv 3	1,855	NE	14	1.0	19	3.7	1.80 / angular
Juv 4	1,780	NNW	8	1.5	94	6.5	2.52 / subangular
Juv 5	1,760	NNW	17	1.9	34	4.8	2.31 / subangular
Juv 6	1,710	NNW	18	1.3	23	3.0	2.30 / subangular
Juv 7	1,680	NNW	17	1.7	38	2.9	2.66 / subangular
Juv 8	1,640	NNW	17	1.8	36	3.3	2.68 / subangular
Juv 9	1,600	NNW	17	2.3	40	3.1	2.59 / subangular
Juv 10	1,690	N	12	1.6	59	5.0	2.45 / subangular
Juv 11	1,660	N	13	1.6	57	4.5	2.38 / subangular
Juv 12	1,620	N	18	1.7	52	3.5	2.41 / subangular
Juv 13	1,755	ESE	6	2.5	35	8.0	2.76 / subangular
Juv 14	1,850	ENE	22	1.0	14	3.2	1.78 / angular
Juv 15	1,865	SE	11	1.3	24	4.2	1.72 / angular
Juv 16	1,865	SSW	12	1.1	12	4.5	1.76 / angular
Juv 17	1,880	NW	5	1.3	41	4.0	2.56 / subangular
Juv 18	1,810	E	5	1.4	17	2.5	2.64 / subangular
Juv 19	1,720	E	13	1.1	29	3.4	2.66 / subangular
Juv 20	1,820	E	6	2.0	17	2.9	2.59 / subangular
Juv 21	1,840	E	12	2.0	38	3.5	2.72 / subangular
Juv 22	1,895	E	7	1.3	43	3.0	2.68 / subangular
Juv 23	1,920	SE	10	1.1	28	3.3	2.81 / subangular

[1] Clast roundness index (see text) and dominant clast roundness category

Table 3

Site	Mean ± 95% CI[1]	σ	Skewness	Kurtosis	Boulders (n)
Juv 1	52.95 ± 1.24	12.69	-0.567	-0.075	400
Juv 2	52.58 ± 1.26	12.91	-0.395	-0.241	400
Juv 3	52.80 ± 1.30	13.24	-0.380	-0.291	400
Juv 4	52.79 ± 1.30	13.28	-0.162	0.214	400
Juv 5	53.38 ± 1.13	11.53	-0.504	-0.192	400
Juv 6	53.91 ± 1.16	11.87	-0.699	0.309	400
Juv 7	55.50 ± 1.10	11.21	-0.689	0.169	400
Juv 8	53.95 ± 1.14	11.67	-0.447	-0.015	400
Juv 9	51.41 ± 1.15	11.73	-0.114	-0.487	400
Juv 10	52.45 ± 1.05	10.68	-0.320	0.082	400
Juv 11	52.66 ± 1.15	11.69	-0.397	-0.403	400
Juv 12	51.84 ± 1.08	11.05	-0.386	-0.394	400
Juv 13	52.70 ± 1.17	11.94	-0.583	0.054	400
Juv 14	53.83 ± 1.09	11.10	-0.443	-0.289	400
Juv 15	52.44 ± 1.17	11.94	-0.305	-0.155	400
Juv 16	52.58 ± 1.22	12.44	-0.381	0.346	400
Juv 17	53.63 ± 1.18	12.06	-0.609	-0.055	400
Juv 18	52.83 ± 1.25	12.74	-0.710	-0.078	400
Juv 19	53.65 ± 1.13	11.48	-0.529	-0.035	400
Juv 20	52.94 ± 1.16	11.80	-0.506	-0.202	400
Juv 21	52.45 ± 1.17	11.95	-0.476	-0.061	400
Juv 22	52.88 ± 1.25	12.79	-0.744	0.151	400
Juv 23	55.07 ± 1.21	12.37	-0.573	-0.138	400
Sorted circles (Winkler et al. 2016)					
Site 2 (1,850 m a.s.l.)	55.03 ± 0.77	10.71	-0.426	-0.203	750
Site 3 (1,750 m a.s.l.)	53.37 ± 0.79	11.02	-0.482	-0.265	750
Site 4 (1,550 m a.s.l.)	51.12 ± 0.86	12.05	-0.216	-0.602	750

[1] Mean of R_{Rock}-values with 95 % confidence intervals ($\alpha = 0.05$).

Table 4

Sites included in analysis (n)	Mean slope angle of sites (°)	R^2-value (linear regression analysis)
23 (all)	no selection	0.027
16	< 15	0.118
12	< 13	0.289
6	< 9	0.408
5[1]	< 9	0.875

[1] Site Juv 22 not included.

Table 5

Locality	Mean ± 95% CI[1]	Boulders (n)	Source
Vesljuvbrean (boulders on foreland exposed c. 2000 CE: 1,840-1,845 m a.s.l.)			
Site y1	75.20 ± 1.01	50	this study
Site y2	76.14 ± 1.00	50	this study
Combined total:	75.67 ± 0.72	100	this study
Storbrean/Leirbrean (bedrock on forelands exposed c. 1900 CE: 1,260/1,510 m a.s.l.)			
Combined total:	76.14 ± 0.67	200	Winkler & Matthews (2014)

[1] Mean R_{Rock}-value with 95 % confidence interval ($\alpha = 0.05$).

Table 6

Locality	Mean ± 95% CI[1]	Boulders (n)	Source
Juvflye (boulders on terminal moraine: c. 1,650 m a.s.l.)			
Site x1.1	46.10 ± 1.46	400	this study
Site x1.2	46.00 ± 1.30	400	this study
Site x1.3	44.48 ± 1.23	400	this study
Combined sites x1.1 + x1.2	46.05 ± 0.98	800	this study
Combined total:	45.53 ± 0.77	1200	this study
Juvflye (bedrock: c. 1,630 m a.s.l.)			
Combined total:	46.53 ± 1.55	200	unpublished data
Leirdalen/Bøverbrean/Leirbrean (bedrock exposed ~9700 ka: c. 1,050/1,400/1,520 m a.s.l.)			
Combined total:	47.88 ± 1.13	300	Winkler & Matthews (2014)

[1] Mean R_{Rock}-value with 95 % confidence interval ($\alpha = 0.05$).

Table 7

SHD-calibration equation		'Young' control point[1]	'Old' control point[2]
Juvflye 1	**y = 24514.357 – 321.70156x**	site y2	sites x1.1+2 (moraine)
Juvflye 2	y = 24098.249 – 316.23652x	site y2	x1 total (moraine)
Juvflye 3	y = 24911.429 – 326.91658x	site y2	x2 (bedrock)
Juvflye 4	y = 24749.426 – 326.80621x	y total	sites x1.1+2 (moraine)
Juvflye 5	y = 24322.777 – 321.16788x	y total	x1 total (moraine)
Juvflye 6	y = 25156.774 – 332.18943x	y total	x2 (bedrock)
Jotunheimen	y = 25931.083 – 338.99505x	Winkler & Matthews (2014)[3]	Winkler & Matthews (2014)

[1] selected local 'young' control point on Juvflye (see Tab. 5)
[2] selected local 'old' control point on Juvflye (see Tab. 6)
[3] control point for RockSchmidt presented by Winkler & Matthews (2014; see Tabs. 5, 6)

Table 8

| Sorted circles[1] | | Age estimate for calibration equation[2]: | | | | | | |
Site	SHD-age (years ago)	Juv 1	Juv 2	Juv 3	Juv 4	Juv 5	Juv 6	Jotunheimen
2	6,910 ± 510	**6,810 ± 245**	6,700 ± 245	6,920 ± 250	6,765 ± 250	6,650 ± 240	6,875 ± 255	7,275 ± 260
3	7,460 ± 540	**7,345 ± 255**	7,220 ± 250	7,465 ± 260	7,310 ± 260	7,180 ± 255	7,430 ± 260	7,840 ± 270
4	8050 ± 560	**8,055 ± 280**	7,915 ± 275	8,185 ± 280	8,025 ± 280	7,890 ± 275	8,160 ± 285	8,585 ± 295

[1] SHD-ages for sorted circle sites published by Winkler et al. (2016). The results were obtained from mechanical Schmidt-hammer data and application of the 'Jotunheimen' calibration equation of Matthews and Owen (2010) only (see text).
[2] Results based on RockSchmidt data collected at the sorted circle sites by Winkler et al. (2016) but not utilised previously for SHD dating (see Tab. 7 for details on calibrations equations).

Table 9

Site	SHD-age estimate (years ago)	Site	SHD-age estimate (years ago)
Juv 1	**7,480 ± 400**	Juv 13	**7,560 ± 375**
Juv 2	**7,600 ± 410**	Juv 14	**7,195 ± 350**
Juv 3	**7,530 ± 420**	Juv 15	**7,645 ± 375**
Juv 4	**7,530 ± 420**	Juv 16	**7,600 ± 395**
Juv 5	**7,340 ± 365**	Juv 17	**7,260 ± 380**
Juv 6	**7,170 ± 375**	Juv 18	**7,520 ± 400**
Juv 7	**6,660 ± 355**	Juv 19	**7,255 ± 360**
Juv 8	**7,160 ± 370**	Juv 20	**7,485 ± 370**
Juv 9	**7,975 ± 370**	Juv 21	**7,640 ± 375**
Juv 10	**7,640 ± 340**	Juv 22	**7,505 ± 405**
Juv 11	**7,575 ± 370**	Juv 23	**6,800 ± 390**
Juv 12	**7,835 ± 350**		

Table 10

(a)

SHD-calibration equation		Age assigned to 'old' control point[1] (years ago)
Juvflye 1	**y = 24514.357 − 321.70156x**	**9,700**
Juvflye 1a	y = 25779.561 − 338.31838x	10,200
Juvflye 1b	y = 27803.888 − 364.90528x	11,000
Juvflye 1c	y = 29575.174 − 388.16883x	11,700

(b)

Site	Calibration equation: Juv 1 (years ago)	Juv 1a	Juv 1b	Juv 1c
Juv 7[2]	**6,660 ± 355**	7,005 ± 370	7,550 ± 400	8,030 ± 425
Juv 9[3]	**7,975 ± 370**	8,385 ± 390	9,045 ± 420	9,620 ± 445

[1] alternative age estimates for the terminal moraine (see text).
[2] sorted stripe site with youngest SHD-age estimate
[3] sorted stripe site with oldest SHD-age estimate

Table captions

Tab. 1. Maximum, minimum, and average mean monthly air temperatures for the meteorological station at Juvvasshøe (1894 m a.s.l.) on Juvflye for September 1999 to August 2019 (data: www.met.no).

Tab. 2. Morphological, sedimentological, and topographical data for the sorted stripe sites investigated on Juvflye. Data for coarse stripe width, length, and distance between coarse stripes constitute average values for those features sampled at each site (for further details see text).

Tab. 3. R_{Rock}-values for the sorted stripe sites on Juvflye. For comparison, the RockSchmidt data for sorted circles from Winkler et al. (2016) are included.

Tab. 4. The increase in value of the coefficient of determination (R^2) from linear regression analysis ($\alpha = 0.05$) between site mean R_{Rock}-value and altitude with decreasing slope angle (see text).

Tab. 5. Mean R_{Rock}-value (± 95 % confidence intervals) for the 'young' control points used for calculation of SHD-calibration equations (see text for details).

Tab. 6. Mean R_{Rock}-value (± 95 % confidence intervals) for the 'old' control points used for calculation of SHD-calibration equations (see text for details).

Tab. 7. Preferred local SHD-calibration equation 'Juvflye 1' (presented in bold) and alternatives based on different selections for the respective 'young' and 'old' control points. The new 'regional' calibration equation exclusively based on the data of Winkler and Matthews (2014) is additionally shown (see text for details).

Tab. 8. SHD-ages for three sorted circles sites on Juvflye (Winkler et al. 2016) compared with the results of both preferred (presented in bold) and alternative calibration equations (see text for further details).

Tab. 9. SHD-ages for sorted stripe sites applying the preferred local calibration equation 'Juvflye 1'.

Tab. 10. (a) Alternatives to the preferred local SHD-calibration equation assuming different ages for the respective 'old' control point. (b) SHD-ages for two selected sorted stripe sites applying the calibration equations presented in (a) (see text for further explanation).

Figure captions

Fig. 1 Study area and location of sorted stripe sites (numbered Juv 1 – 23) investigated on Juvflye in Jotunheimen, central South Norway. Locations of 'young' (y) and 'old' control points (x) for the SHD-calibration equation are indicated (see 3.3 for details).

Fig. 2. Sorted stripes on Juvflye. (a) View from site Juv 15 in northeasterly direction towards Storslokkje and Svartkampan (see Figure 1; photo: July 2019); (b) View from Juvvasshøe in southerly direction towards Juvvashytta and Galdhøpiggen Sommerskisenter (far distance; photo: July 2018); (c) – (g) Orthorectified aerial photo (2017) of sorted stripes around sites Juv 11 (c), Juv 8 (d), Juv 23 (e), Juv 13 (f), and at the southern slope of Juvflye descending towards the glacier foreland of Styggebrean including site Juv 23 (g). Aerial photography adapted from www.norgeibilder.no, © Kartverket/www.kartverket.no.

Fig. 3. Selected sorted stripe sites on Juvflye. (a) Juv 3; (b) Juv 9; (c) Juv 11; (d) Juv 14; (e) Juv 22, (f) Juv 23. All photos: July 2019.

Fig. 4. Small solifluction lobes in the fine-grained terrain between coarse stripes at site Juv 8. Both photos: July 2019.

Fig. 5. Mean R_{Rock}-value (± 95 % confidence intervals) for each subsample (n = 20) from selected individual coarse stripes with at least 10 subsamples each. The data reflect consecutive sampling from the top of each stripe in the downslope direction.

Fig. 6. Histograms of R_{Rock}-values for selected sites.

Fig. 7. Site mean R_{Rock}-values (± 95 % confidence intervals) for all sorted stripe sites on Juvflye in relation to aspect.

Fig. 8. Site mean R_{Rock}-value plotted against different topographical (altitude (a), slope angle (b)), morphological (coarse stripe width (c), length (d), distance (e)), and sedimentological parameters (*ir* (f)). The coefficient of determination (R^2) from linear regression analysis ($\alpha = 0.05$) is given.

Fig. 9. SHD-ages and related errors for all sorted stripe sites investigated on Juvflye based on local calibration equation 'Juvflye 1' and arranged according to their altitude. The roman numbers and the

shading refer to regional neoglacial events (Smørstabbtindan I – VII) documented by Matthews and

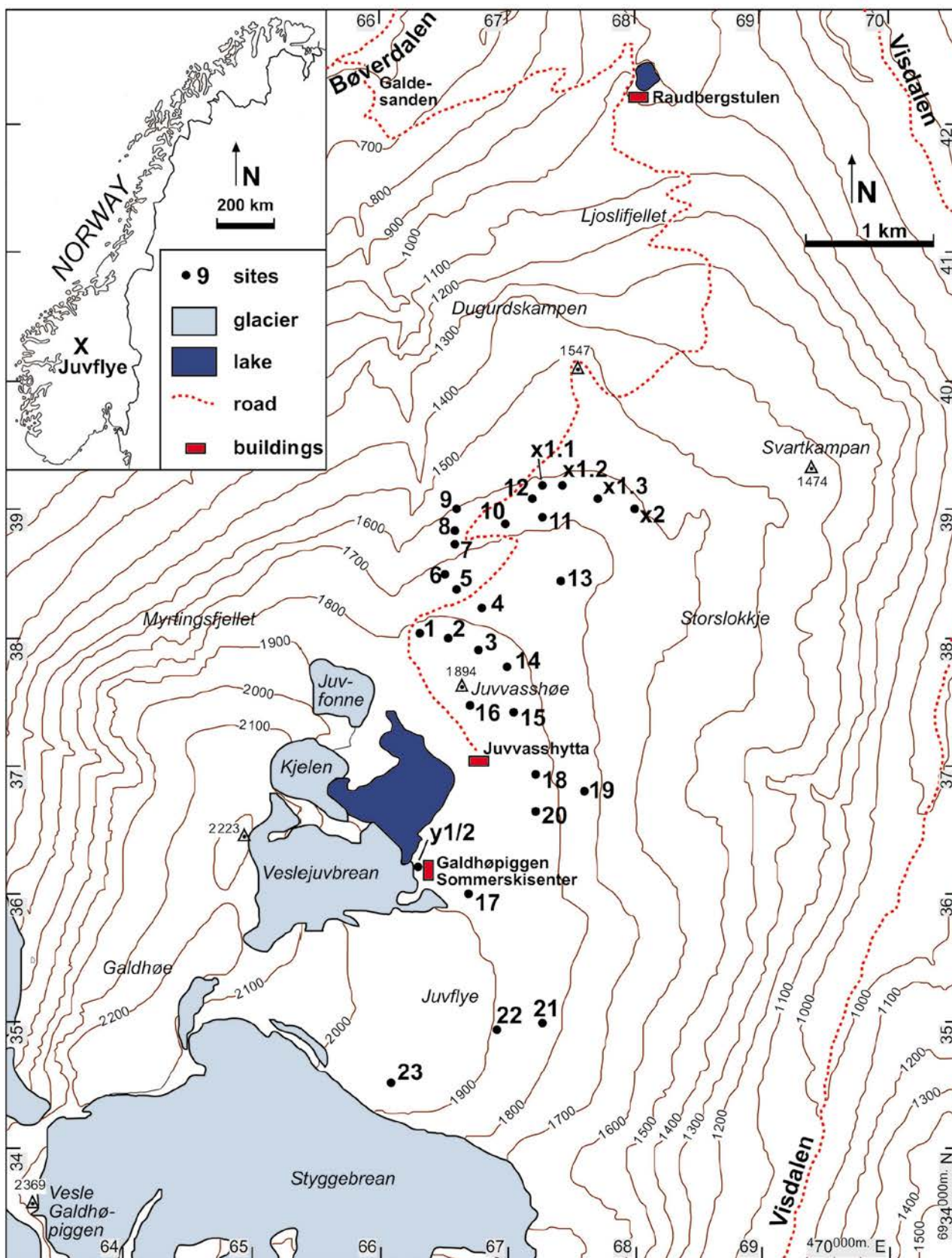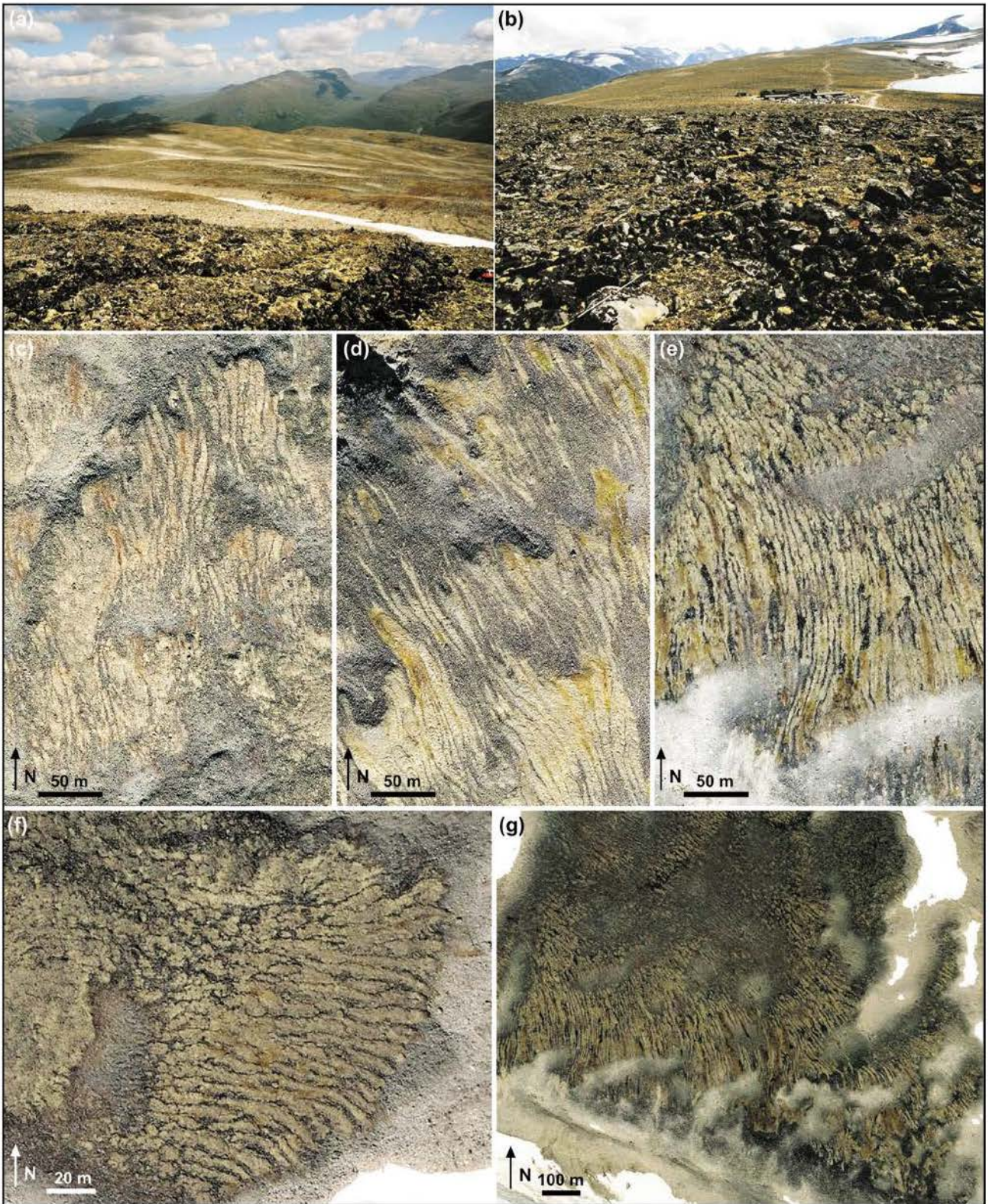Dresser (2008) in the nearby Smørstabbtindan Massif in Jotunheimen.
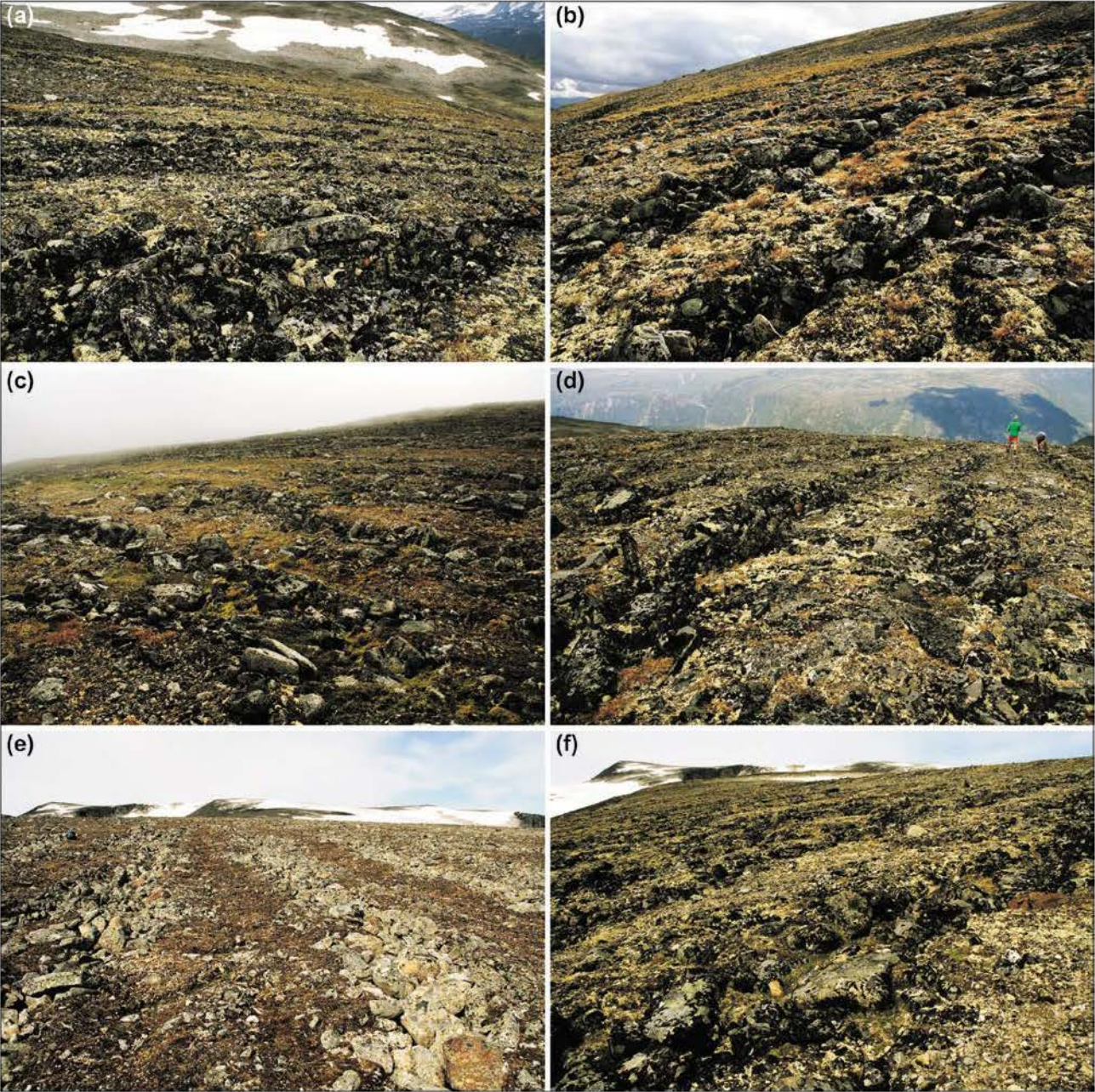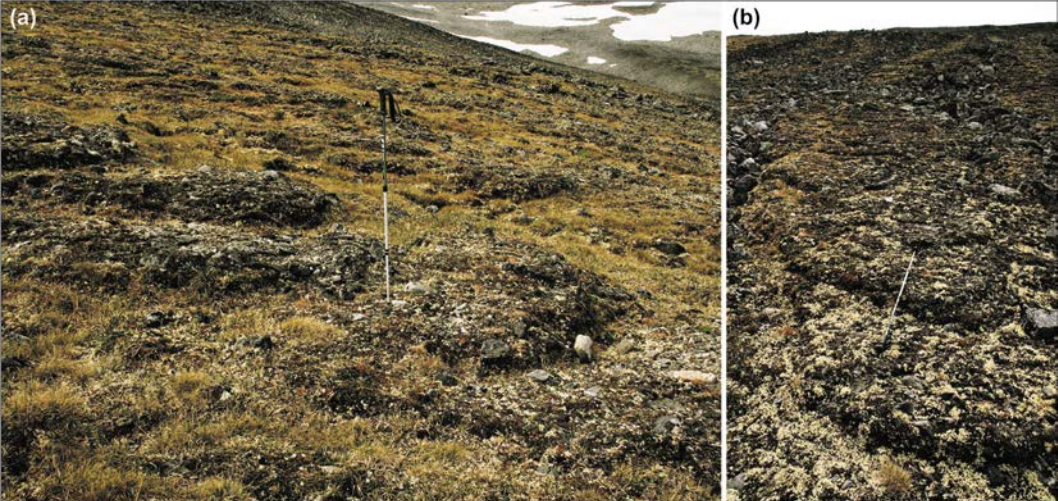
Fig.1

Fig.2

Fig.3

Fig.4

Fig.5

Fig.6

Fig.7

Juvflye - all sites sorted by aspect

Fig.8

Fig.9